Tunnelling and Underground Space Technology 176 (2026) 107885

Contents lists available at ScienceDirect

Tunnelling and Underground Space Technology incorporating Trenchless Technology Research

journal homepage: www.elsevier.com/locate/tust

Evaluation of ground-motion intensity measures for seismic response of fault-crossing tunnels

Chao Luo [a,b], Haowei Du [b], Yanliang Du [c,d], Xiangbo Bu [e], Fei Xu [c,d,*], Hemin Zheng [f,g], Hao Wang [a,b], Zerui Ji [b]

[a] Key Laboratory of Roads and Railway Engineering Safety Control, Ministry of Education, Shijiazhuang Tiedao University, Shijiazhuang 050043, China
[b] School of Civil Engineering, Shijiazhuang Tiedao University, Shijiazhuang 050043, China
[c] Key Laboratory of Large Structural Health Monitoring and Control, Shijiazhuang Tiedao University, Shijiazhuang 050043, China
[d] Yanzhao Modern Transportation Laboratory, Shijiazhuang 050043, China
[e] School of Safety Engineering and Emergency Management, Shijiazhuang Tiedao University, Shijiazhuang 050043, China
[f] School of Qilu Transportation, Shandong Univ., Jinan 250002, China
[g] China Railway Design Group Co., Ltd., Tianjin 300308, China

ARTICLE INFO

Keywords:
Seismogenic-fault-crossing tunnels
Tunnel engineering
Shaking table test
Ground-motion intensity measures
Fault displacement (fault slip)
Seismic response of structures

ABSTRACT

Seismic damage mechanisms of fault-crossing tunnels are complex and involve the coupled effects of fault offset and seismic ground-motion. Accurately characterizing seismic demand for such tunnels remains challenging due to the limitations of conventional ground-motion intensity measures. In this study, a series of shaking table tests is conducted to investigate the applicability of different ground-motion intensity measures (IMs) for evaluating the seismic response of fault-crossing tunnels. Both absolute-motion-based and relative-motion-based IMs are examined, and their performance is assessed in terms of response ranking consistency and correlation with tunnel lining strain demand. The experimental results show that absolute-motion-based IMs exhibit limited capability in consistently ranking tunnel response and correlating with lining strain demand under fault-crossing excitation. Relative-motion-based IMs provide improved performance; however, individual relative IMs exhibit distinct trade-offs between response ranking and correlation with response magnitude. Based on these findings, a multi relative-motion-based IM framework is proposed by combining a ratio-type IM with displacement-related IMs to jointly represent deformation characteristics and intensity levels. Within the scope of the present shaking table tests, the proposed framework provides an experimentally supported and physically interpretable approach for characterizing fault-crossing seismic demand and offers a useful reference for ground-motion selection in the seismic analysis of fault-crossing tunnels.

1. Introduction

Ground-motion intensity measures (IMs) play a crucial role in earthquake engineering by providing a quantitative link between seismic hazard and structural demands (Cornell 1968). The selection of appropriate IMs directly affects the reliability of probabilistic seismic demand models, fragility analyses, and seismic risk evaluation (Moehle et al., 2004). For above-ground structures, decades of research have established relatively mature IM frameworks, in which spectral acceleration and other scalar or vector IMs have been shown to efficiently predict structural responses under a wide range of seismic excitations.

Accordingly, investigating the relationship between IMs and structural responses has long been a central research topic in earthquake engineering. For above-ground structures, ground-motion intensity measures have been extensively investigated and incorporated into relatively mature probabilistic seismic performance frameworks. Luco et al. (Luco and Cornell, 2007) established a probabilistic framework for structure-specific scalar intensity measures, clarifying the bridging role of IMs in linking seismic hazard to structural demand prediction. Cornell et al. (Cornell et al., 2002) further introduced spectral acceleration as the primary IM into performance-based earthquake engineering, enabling the probabilistic evaluation of structural performance by explicitly accounting for uncertainties in ground-motion intensity, structural demand, and structural capacity. Subsequent studies

* Corresponding author.
E-mail address: xufei@stdu.edu.cn (F. Xu).

https://doi.org/10.1016/j.tust.2026.107885
Received 11 March 2026; Received in revised form 22 May 2026; Accepted 16 June 2026

demonstrated that the predictive efficiency of IMs strongly depends on the dynamic characteristics of the structure. Baker (Baker, 2007) conducted a comprehensive statistical analysis of correlations among commonly used IMs and showed that different IMs exhibit marked differences in suitability for predicting structural and geotechnical responses. By introducing elastic spectral-shape information, Vamvatsikos et al. (Vamvatsikos and Cornell, 2005) developed efficient scalar and vector IMs (using two intensity measures) for predicting interstory drift ratios, substantially reducing the dispersion of nonlinear response predictions in incremental dynamic analysis. Iervolino et al. (Iervolino and Cornell, 2005) demonstrated the robustness of IMs as a unified scaling basis for record selection, showing that they can streamline the ground-motion selection procedure without reliance on specific magnitude–-distance scenarios. It is widely recognized that spectral acceleration offers high predictive efficiency for most building structures, whereas velocity- and displacement-related measures tend to perform better for long-period structures or in strongly nonlinear response regimes (Baker and Jayaram, 2008). Overall, a relatively mature theoretical framework for IMs has been established for above-ground structures. However, their effectiveness relies on the fact that structural response is predominantly inertia-controlled and can be adequately characterized using absolute ground-motion records at a single location.

For underground structures, seismic demand is governed by fundamentally different mechanisms from those of above-ground systems. Early studies by Wang (Wang, 1993) and Penzien (Penzien, 2000) indicate that damage in underground structures is predominantly deformation-controlled, and their responses are more closely related to free-field ground deformations rather than inertial forces. Hashash et al. (Hashash et al., 2001) provided a systematic synthesis of seismic response characteristics of underground structures, noting that directly adopting IMs commonly used for above-ground structures may not adequately represent seismic demand in underground systems. Tsinidis (Tsinidis, 2017) reported that the seismic response of rectangular tunnels is primarily controlled by soil shear deformation; consequently, tunnel internal forces and deformations exhibit weak correlation with acceleration-based IMs such as peak ground acceleration, whereas velocity- and displacement-related IMs provide more representative and stable descriptors of underground structural response. Based on probabilistic seismic demand analysis of metro-station structures, Zhang et al. (Zhang et al., 2023) showed that conventional PGA is ineffective in reliably predicting underground seismic demand; in contrast, spectral-shape IMs compatible with the structural dynamic characteristics, as well as velocity- and displacement-based IMs, achieve higher predictive efficiency and lower dispersion in estimating internal forces and deformations. In the seismic performance assessment of rectangular tunnels by Nguyen et al. (Nguyen et al., 2023), velocity spectrum intensity was identified as the optimal IM, exhibiting the strongest correlation with tunnel damage, the highest efficiency, and the best overall performance. These studies collectively suggest that, for underground structures, IMs reflecting ground deformation and cumulative motion characteristics are generally more suitable than acceleration-based measures.

In the specific context of shield tunnels in complex soil conditions, Shen et al. (Shen et al., 2025) conducted a scalar- and vector-valued seismic fragility assessment of segmental shield tunnel linings in liquefiable soil deposits, highlighting the complexity of segmented systems. Concurrently, Shen et al. (Shen et al., 2025) systematically evaluated 23 candidate IMs using nonlinear dynamic effective stress analyses. Their results revealed that for shield tunnels in both liquefiable and non-liquefiable soils, sustained maximum acceleration (SMA) and PGA are the most proficient IMs, challenging the generalizability of earlier conclusions derived mainly from rectangular structures. However, most existing investigations implicitly assume that seismic demand can be characterized using absolute ground-motion records at a single location, an assumption that may not hold for underground structures subjected to spatially non-uniform ground deformation.

In the case of underground structures crossing active seismogenic faults, the limitations of conventional IM frameworks become even more pronounced. Fault-crossing tunnels are subjected not only to transient seismic shaking, but also to permanent ground deformation and differential displacement across the fault zone. The resulting structural demand is therefore controlled by the relative motion between the two sides of the fault, rather than by the absolute motion at a single point. However, existing studies on fault-crossing underground systems remain limited and are predominantly focused on buried pipelines. O'Rourke et al. (O'Rourke and Liu, 2012) pointed out that conventional IMs represented by peak ground acceleration are unable to capture the effects of permanent ground deformation caused by fault displacement. Bray et al. (Bray and Travasarou, 2007) and Karamitros et al. (Karamitros et al., 2007) further showed that permanent-displacement measures and velocity-related IMs possess clearer physical relevance for characterizing the response of fault-crossing pipelines. While these findings provide valuable insights, a systematic evaluation of IMs for fault-crossing tunnels—particularly from an experimental perspective that explicitly accounts for fault-side relative motion—is still lacking.

Despite the growing body of research on intensity measures for underground structures, a critical gap remains in the context of tunnels crossing active seismogenic faults. Existing studies have predominantly focused on either underground structures subjected to uniform ground shaking or experiencing fault rupture. For fault-crossing tunnels, the seismic demand arises from the combined effects of transient shaking and permanent ground deformation, resulting in highly non-uniform ground-motion along the tunnel axis. Consequently, the applicability of conventional IMs—largely derived from absolute ground-motion records at a single location—remains unclear for fault-crossing tunnels, where relative motion across the fault plays a critical role. Moreover, systematic experimental investigations that explicitly incorporate fault-side differential displacement and quantitatively evaluate the predictive performance of different IMs are still scarce. The lack of such studies limits the development of rational IM-based frameworks for seismic demand assessment and ground-motion selection in the design of fault-crossing tunnels.

This study aims to evaluate the applicability of ground-motion intensity measures for tunnels crossing active seismogenic faults, with explicit consideration of fault-induced relative motion. Using shaking table tests of a tunnel model crossing a dual-fault system, the relationships between strain demands and various intensity measures derived from relative-motion time histories are systematically investigated. The results of this work are expected to enhance the understanding of seismic demand characteristics of fault-crossing tunnels and to support more rational selection of ground motions in seismic design. By highlighting the importance of relative motion and displacement-related IMs, the study provides experimental insight into the seismic performance assessment, seismic fragility analysis and design of underground structures subjected to fault-crossing ground motions.

2. Experimental program

The detailed design of the shaking table test program, including model configuration, material selection, and construction procedures, has been reported in a separate publication (Xu et al., 2026). The shaking-table test program is summarized below, with emphasis on the experimental details directly relevant to the evaluation of tunnel lining strain response and ground-motion intensity measures.

2.1. Engineering background and fault-crossing scenario

The experimental study is motivated by a tunnel project crossing an active seismogenic fault zone characterized by complex fault geometry and multiple fault branches. The fault system considered in this study consists of two major branches, denoted as F9 and F10, which intersect the tunnel alignment at different locations, as shown in Fig. 1. Fault F9

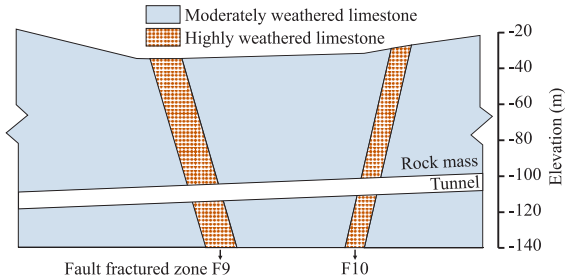

Fig. 1. Fault diagram(Xu et al., 2026).

has an approximate width of 10 m and a dip angle of about 83°, while fault F10 is approximately 20 m wide with a dip angle of about 75°. The fractured zones are predominantly composed of fault breccia and cataclasite and are classified as Grade V surrounding rock, and the hanging wall and footwall mainly consist of slate and granite and are classified as Grade IV surrounding rock. This geological setting provides a representative scenario for investigating the seismic response of tunnels subjected to fault-induced differential motion. This dual-fault configuration allows different fault-rupture scenarios to be reproduced experimentally and provides a suitable basis for examining tunnel response under fault-induced relative motion.

2.2. Shaking table test facility

The shaking table tests were conducted on the shaking table array at the Engineering Earthquake Resistance Research Center of Guangzhou University. As shown in Fig. 2, the array consists of one 8 m × 10 m shaking table (Table 1 in Fig. 2) and two 4 m × 4 m shaking tables (Tables 2 and 3 in Fig. 2), all of which are three-directional, six-degree-of-freedom (6-DOF) systems. The test facility is shown in Fig. 2. This configuration enables the application of independent but synchronized seismic inputs to different segments of the tunnel model, thereby allowing the simulation of fault-induced relative motion across multiple fault interfaces.

In the present study, the tunnel model was arranged longitudinally across the three shaking tables. The interfaces between adjacent tables were used to represent the locations of Faults F9 and F10, respectively. By prescribing different input motions to the adjacent shaking tables, seismic scenarios of tunnels subjected to fault-crossing ground motions can be reproduced in a controlled manner.

The three shaking tables were driven by independent, non-uniform seismic inputs, enabling the tunnel model to experience spatially varying ground motions associated with fault-crossing scenarios. The key performance parameters of the shaking tables, including payload capacity, acceleration limits, and operating frequency ranges, were sufficient to meet the requirements of the scaled tunnel model and the input ground motions considered in this study.

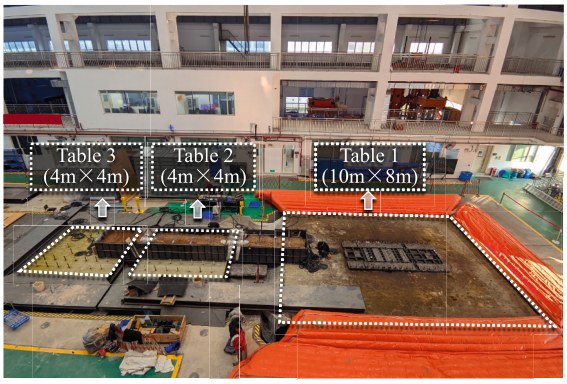

Fig. 2. Shaking table array(Xu et al., 2026).

Table 1
Similarity relationship and similarity ratio.

Physical quantity	Similarity relation	Design similarity ratio	Actual similarity ratio
Geometric dimensions	C_l(basic similarity ratio)	1/50	1/50
Time	$C_t = C_l\sqrt{C_\rho/C_E}$	$1/5\sqrt{2}$	1/7
Modulus of elasticity	C_E(basic similarity ratio)	0.018	0.018
Cohesion	$C_C = C_E$	0.018	0.0175
Angle of friction	C_φ	1	1
Acceleration	C_a(basic similarity ratio)	1	1
Density	$C_\rho = C_E\sqrt{C_l/C_a}$	0.9	0.7
Frequency	$C_f = 1/C_t$	7	7
Strain	C_ε	1	1
Displacement	$C_d = C_l$	1/50	1/50
Stress	$C_\sigma = C_E$	0.018	0.018

Table 2
Specific physical and mechanical parameters of surrounding rock.

Material	Type	Density ρ/(g·cm^{-3})	Cohesion c/kPa	Angle of internal friction φ/(°)	Modulus of elasticity E/MPa
Surrounding rock	Prototype actual value	2.4	650	37	6000
	Model theoretical value	1.6	10.8	37	100
	model actual value	1.68	11.4	38	108
Fault	Prototype actual value	2.2	180	24	1100
	Model theoretical value	1.46	3.0	24	18
	model actual value	1.63	3.2	26	17

2.3. Similarity relationships

To ensure that the scaled tunnel model can adequately reproduce the seismic response characteristics of the prototype tunnel, similarity relationships were established based on similitude theory. Considering that the seismic behavior of underground structures is predominantly deformation-controlled, the geometric similarity ratio was selected as the primary controlling parameter.

Based on the selected similarity framework, the similarity ratios of key physical quantities, including geometric dimensions, elastic modulus, stress, strain, and displacement, were determined. The adopted similarity relationships and corresponding similarity ratios are summarized in Table 1 and form the basis for the subsequent analysis of tunnel lining strain response under fault-crossing ground motions.

It should be noted that Table 1 reports both the design similarity ratios and the actual similarity ratios. The design similarity ratios are the target values determined according to the similitude law, whereas the actual similarity ratios were calculated from the measured properties of the model materials. The frequency similarity ratio is 7.0 for both the design and actual values, indicating that the frequency similitude was maintained in the test. The difference in the cohesion similarity ratio is small, changing from 0.018 in the design value to 0.0175 in the actual

Table 3
Specific physical and mechanical parameters of similar materials for tunnel model.

Type	Density ρ/(g·cm^{-3})	Modulus of elasticity E/MPa	Poisson's ratio	Tensile strength MPa	Compressive Strength MPa
Prototype actual value	2.42	34,500	0.2	2640	32,400
Model theoretical value	1.61	575	0.2	44	540
model actual value	1.50	523	0.2	41	457

value, and this minor deviation is not expected to significantly affect the overall stress–strain similitude.

In contrast, the density similarity ratio shows a relatively larger deviation, with a design value of 0.9 and an actual value of 0.7. This discrepancy may influence inertia-related quantities, dynamic stress levels, wave impedance, and the absolute amplitude of wave propagation. Therefore, the shaking table model should be regarded as satisfying the similitude requirements approximately rather than exactly. In the present study, the main objective is to evaluate the relative effectiveness of different IMs under the same model configuration and material similitude conditions, rather than to directly reproduce a unique prototype response in an absolute sense. Accordingly, although the density discrepancy may affect the absolute response amplitude, it is expected to have a limited influence on the relative ranking and comparative evaluation of different IMs. This limitation should be considered when extending the present results to prototype-scale engineering applications.

2.4. Similitude materials and seismic mitigation configuration

The tunnel lining model was fabricated using a composite similitude material selected to reproduce the deformation characteristics of the prototype lining under seismic loading. The mechanical properties of the adopted material were designed to ensure that lining strain response could be reliably captured under fault-crossing ground motions, which is essential for subsequent correlation analyses between ground-motion

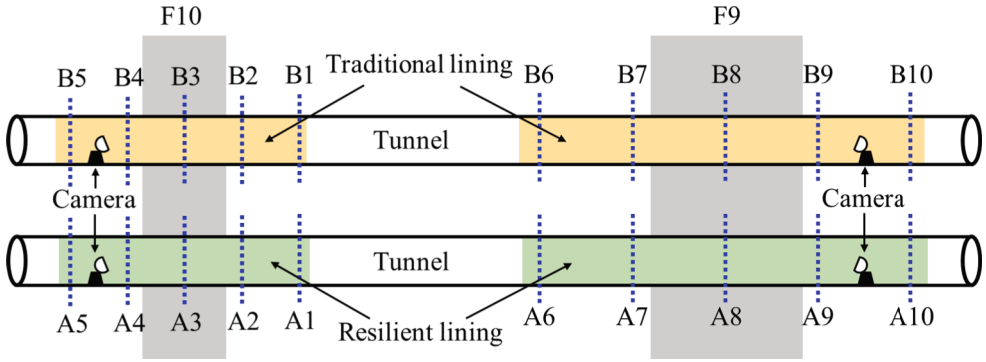

(a) Strain gauge monitoring section

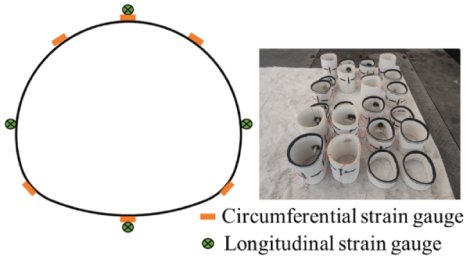

(b) Strain gauge

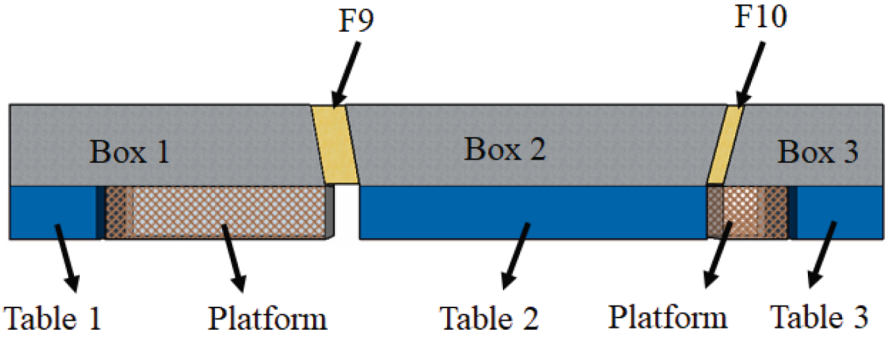

(c) The relative position relationship between the tunnel and the shaking table

Fig. 3. Shaking table test sensor layout(Xu et al., 2026).

intensity measures and structural response. The physical and mechanical parameters of the surrounding rock for both the prototype and the model are listed in Table 2.

Two tunnel lining configurations were considered in the shaking table tests: a conventional lining with rigid connections between segments and a seismic-mitigation lining incorporating flexible joints and an external damping layer. The flexible joints were intended to accommodate fault-induced relative displacement and rotation between adjacent lining segments, while the damping layer was introduced to reduce localized deformation demand in the fault-crossing region. The physical and mechanical properties of the similitude lining material are summarized in Table 3.

The comparison between the two lining configurations under identical fault-crossing seismic inputs provides a consistent basis for evaluating the influence of ground-motion intensity measures on the seismic response of both mitigated and unmitigated tunnel systems.

2.5. Instrumentation and measurement strategy

To capture the seismic response characteristics of the tunnel lining under fault-crossing ground motions, strain was selected as the primary response quantity in the shaking table tests. As shown in Fig. 3, 20 monitoring sections were arranged along the longitudinal direction of the tunnel model, denoted as A1–A10 and B1–B10. Sections A1–A10 correspond to the seismic-mitigation lining with flexible connections, whereas Sections B1–B10 correspond to the conventional lining with rigid connections.

Each monitoring section was instrumented with both longitudinal and circumferential strain gauges. The green points in Fig. 3 represent longitudinal strain gauges, which were used to measure the strain component along the tunnel axis. The orange points represent circumferential strain gauges, which were used to measure the strain component along the circumferential direction of the lining. These gauges were arranged at representative positions of the lining cross-section, including the crown, spandrels, sidewalls, and invert, so that the local deformation characteristics and strain concentration of the tunnel lining near the fault-crossing regions could be captured.

To characterize the spatial variation of lining response associated with fault-induced relative motion, selected monitoring sections were located within and adjacent to the simulated fault zones. In particular, Sections A3 and A8 were positioned across the fault interfaces to capture strain demand in the seismic-mitigation lining, while Sections B3 and B8 served as their counterparts for the conventional lining. This arrangement enables direct comparison of strain response between the two lining configurations under identical fault-crossing seismic inputs.

At each monitoring section, strain gauges were installed to measure both circumferential and longitudinal strain components. Circumferential strain was recorded at representative locations including the crown, shoulders, springlines, and invert, while longitudinal strain was measured at the crown, haunches, and invert. This instrumentation strategy enables the dominant strain components and their spatial distribution along the lining to be captured, providing a consistent basis for evaluating peak strain demand under different ground-motion intensity levels.

The recorded strain time histories were subsequently processed to extract peak strain responses at each monitoring location, which were used as the structural response metrics in the correlation and regression analyses with ground-motion intensity measures presented in Section 3.

3. Selection of input ground motions

3.1. Fault-rupture scenarios and input strategy

To investigate the seismic response of tunnels subjected to fault-crossing ground motions, a set of fault-rupture scenarios was defined based on the dual-fault configuration described in Section 2. Two fault branches, denoted as F9 and F10, intersect the tunnel alignment at different locations, allowing both single-fault and multi-fault rupture conditions to be considered.

In the shaking table tests, the tunnel model was arranged longitudinally across a three-table shaking table array. The interfaces between adjacent shaking tables were used to represent the locations of Faults F9 and F10, respectively. Specifically, the interface between Tables 1 and 2 corresponds to Fault F9, while the interface between Tables 2 and 3 represents Fault F10. This physical mapping enables fault-induced relative motion to be introduced at prescribed locations along the tunnel model.

Based on this configuration, three representative fault-rupture scenarios were considered: (i) rupture of Fault F9 only, (ii) rupture of Fault F10 only, and (iii) simultaneous rupture of both faults. The fault parameters for the single-rupture scenarios of F9 and F10 are summarized in Table 4. The rupture length and rupture width listed in Table 4 were estimated from the target moment magnitude using the empirical magnitude–rupture scaling relationships proposed by Wells and Coppersmith (1994). (Wells and Coppersmith, 1994) By prescribing independent, non-uniform seismic inputs to the three shaking tables, these scenarios can be reproduced in a controlled manner, allowing the tunnel model to experience fault-crossing ground motions characterized by differential displacement across one or multiple fault interfaces. In addition to the simulated ground motions for the above fault-rupture scenarios, two sets of recorded across-fault ground motions were also selected to represent realistic fault-crossing seismic excitations. Together, the simulated and recorded motions constitute five ground-motion cases used in the shaking table tests.

The defined input strategy provides a consistent framework for examining how tunnel lining response varies with the location and extent of fault-induced relative motion, which forms the basis for the subsequent selection and evaluation of ground-motion intensity measures.

3.2. Ground-motion sets and data sources

A total of five ground-motion cases were adopted in the shaking table tests, comprising three sets of simulated fault-rupture ground motions and two sets of recorded near-fault ground motions. The combined use of simulated and recorded motions enables both controlled representation of specific fault-rupture scenarios and incorporation of realistic characteristics observed in actual earthquakes.

3.2.1. Simulated fault-rupture ground motions

The simulated ground motions were obtained using deterministic and physics-based broadband ground-motion simulation methods to numerically realize the fault-rupture scenarios defined in Section 2.1 (Luo and Cao, 2024; Petrone et al., 2021; Pitarka et al., 2020; Rodgers et al., 2020). Unlike recorded ground motions, which represent specific realizations of actual earthquakes and inherently include the combined effects of source rupture, propagation path, local site conditions, and recording-site characteristics, simulated motions are scenario-oriented numerical realizations generated from prescribed source, path, and site models. Therefore, they are not intended to reproduce a particular observed record point by point, but to provide physically constrained three-component time histories that are consistent with the target fault-rupture scenarios and can cover cases for which suitable recordings are unavailable. The reliability of this type of broadband simulation has been supported by the Graves–Pitarka (GP) validation studies. Graves and Pitarka demonstrated that the hybrid broadband simulation framework, which combines deterministic low-frequency wave propagation with semi-stochastic high-frequency radiation, can reproduce the main characteristics of recorded strong motions from the Imperial Valley, Loma Prieta, Landers, and Northridge earthquakes, including PGA, PGV, spectral acceleration, duration, and near-fault directivity effects (Graves and Pitarka, 2010). Subsequent refinements implemented in

Table 4
Parameters of Faults F9 and F10.

Fault	Focal Depth	Rupture Length	Rupture Width	Magnitude	Strike	Dip	Rake
F9	4.8 km	24.5 km	9.3 km	M_w6.79	306.3°	78°	0°
F10	4.6 km	24.5 km	9.3 km	M_w6.79	126.3°	80°	180°

GP14.3 improved the transition between the low- and high-frequency components and reduced the previously identified overprediction of long-period motions, especially in the 2–5 s period range (Graves and Pitarka, 2015). More recently, Graves further validated the GP method through a grid-search analysis of 12 California and Baja California earthquakes, with 240 rupture realizations generated for each event and evaluated against near-fault strong-motion records using pseudo-spectral acceleration goodness-of-fit metrics (Graves, 2022). On this basis, the simulated motions used in this study can be regarded as observation-tested and physically constrained artificial ground motions rather than direct substitutes for individual real earthquake records. For each scenario, three-component ground-motion time histories were generated at the tunnel site and applied to the corresponding shaking tables according to the fault–table mapping.

3.2.2. *Recorded across-fault ground motions*

In addition to the simulated fault-rupture ground motions, two sets of recorded across-fault ground motions were selected from the 1999 Chi-Chi earthquake and the 1979 Imperial Valley earthquake. These two events were adopted because they provide representative real-earthquake records associated with different faulting mechanisms. The Chi-Chi earthquake is characterized by thrust faulting, whereas the Imperial Valley earthquake is dominated by strike-slip faulting. Therefore, the use of these two events allows the experimental input motions to cover typical fault-crossing excitation characteristics produced by different seismogenic fault mechanisms, rather than relying solely on numerically simulated scenarios.

The recorded across-fault motions were selected according to the following principles. First, the selected records were required to be obtained from stations located on opposite sides of the causative fault, so that the differential motion across the fault could be explicitly represented. Second, the records were required to contain clear displacement-related characteristics, including relative displacement or permanent displacement components, because the seismic demand of fault-crossing tunnels is mainly governed by the relative motion between the two sides of the fault rather than by the absolute motion at a single station.

For each event, ground-motion records obtained from stations located on opposite sides of the causative fault were employed as inputs to adjacent shaking tables, enabling across-fault ground-motion input conditions to be reproduced.

Fig. 4 illustrates the displacement time histories of the five ground-motion cases applied to the three shaking tables, highlighting the differences in relative displacement characteristics associated with the various fault-rupture scenarios and recorded across-fault motions.

To characterize fault-crossing seismic excitation, the relative motion across a fault interface is defined as the difference between the displacement time histories applied to the two shaking tables on either side of that interface. Accordingly, the relative displacement time histories across Faults F9 and F10 were obtained from the displacement records of shaking tables 1–2 and shaking tables 2–3, respectively.

For each ground-motion case, the relative displacement time history is computed for both fault interfaces, and its peak value can be used to quantify the magnitude of fault-induced differential motion. This definition allows the contribution of fault-crossing effects to be isolated from absolute ground-motion at a single table. Based on the magnitude of relative displacement across the two interfaces, the causative fault for a given input case was identified as the fault exhibiting the larger relative displacement. This criterion provides a consistent basis for distinguishing whether tunnel response is primarily governed by motion across Fault F9, Fault F10, or both faults acting simultaneously.

To illustrate the identification procedure, the low-intensity excitation level was used as a representative example. The maximum relative displacements across Faults F9 and F10 for the five ground-motion cases are summarized in Table 5. For cases in which significant relative displacement occurred across both interfaces, the corresponding excitation was classified as a multi-fault rupture scenario, whereas cases dominated by relative motion across a single interface were classified as single-fault rupture scenarios.

In this study, two types of ground-motion time histories are distinguished: absolute ground motions and relative ground motions. Absolute ground motions refer to the acceleration, velocity, or displacement time histories directly imposed on an individual shaking table. They represent the seismic input at a single location or on one side of the fault. Accordingly, absolute-motion-based IMs are calculated from the ground-motion record of a single table and describe the intensity level of the local input motion.

Relative ground motions, in contrast, are defined as the differential motion between the two sides of a fault interface. For the present three-table shaking table system, the relative motion across Fault F9 is obtained from the difference between the input motions of Tables 1 and 2, whereas the relative motion across Fault F10 is obtained from the difference between the input motions of Tables 2 and 3.

In the calculation of IMs in this study, the relative motion is evaluated component by component in the same coordinate system. That is, the displacement, velocity, and acceleration histories in the same direction on the two sides of the fault are subtracted at each time step. It is obtained from the time-history difference of corresponding directional components across the fault interface.

The above characterization establishes a clear link between the applied ground motions and the locations of fault-induced relative displacement along the tunnel model, thereby providing the physical basis for subsequent evaluation of ground-motion intensity measures and tunnel lining strain response.

In summary, five ground-motion cases, including three simulated fault-rupture motions and two recorded across-fault motions, were applied to the three shaking tables to reproduce fault-crossing seismic excitation. The defined input motions provide the basis for examining the seismic response of the tunnel lining and for evaluating the applicability of different ground-motion intensity measures in the following sections.

4. Experimental results and analysis

This section presents the experimental results and analysis of the seismic response of the fault-crossing tunnel model. The spatial characteristics of lining strain response are first examined to identify the dominant deformation patterns induced by fault-crossing ground motions. Subsequently, the applicability of different ground-motion intensity measures is evaluated by comparing their ability to characterize tunnel lining strain demand under both simulated and recorded fault-crossing excitations.

4.1. *Spatial distribution of lining strain response*

Based on the shaking table model test results, Fig. 5 presents the spatial distribution of peak lining strain along the longitudinal direction of the tunnel for the low-intensity excitation cases. For all excitation cases, the lining strain exhibits a strongly non-uniform distribution, with

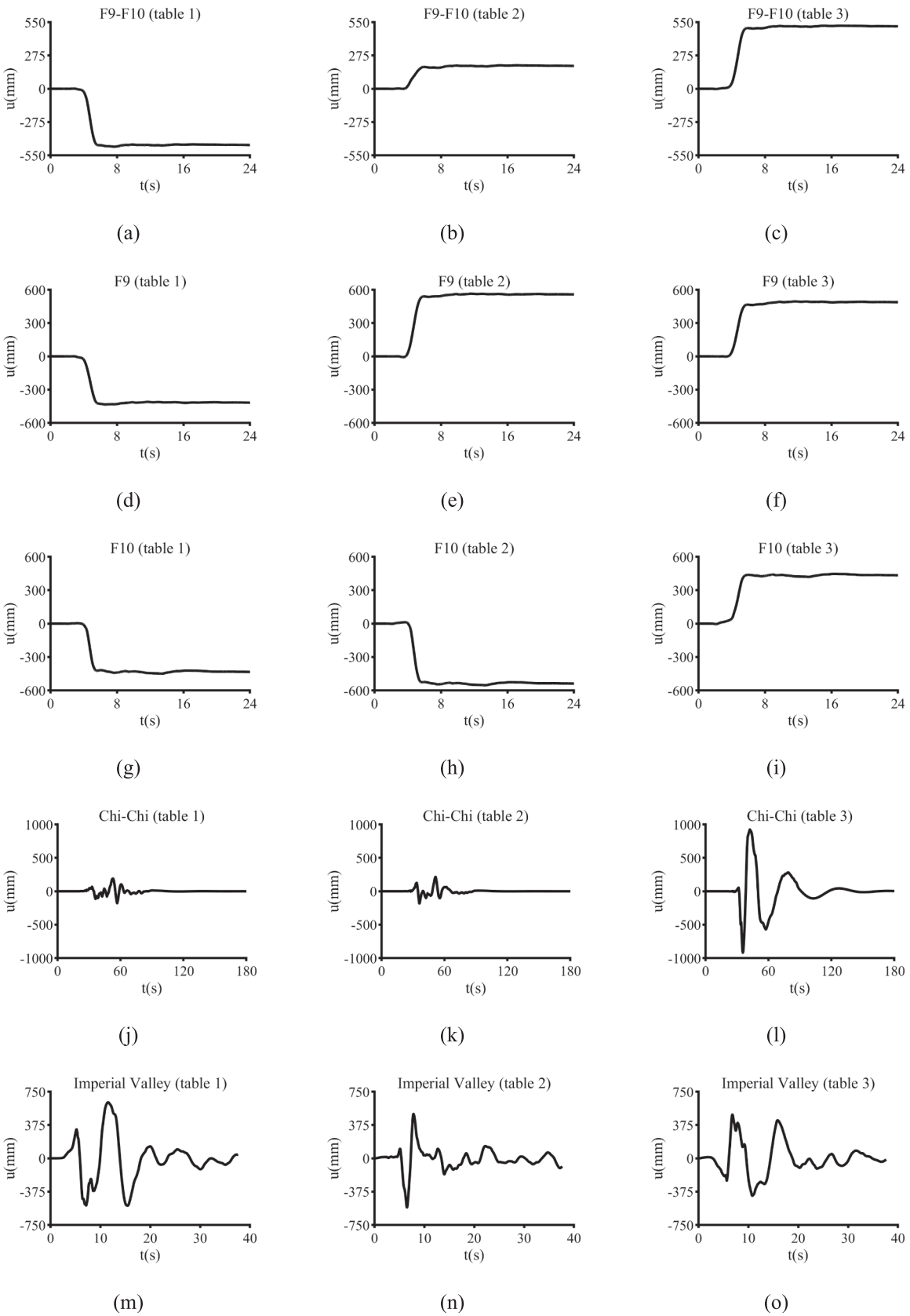

Fig. 4. Displacement time histories of seismic ground motions applied to the three shaking tables under different input cases.

Table 5
Maximum relative displacement (mm) of five types of earthquakes on two faults.

Fault	F9-F10	F9	F10	Chi-Chi	Imperial Valley
1–2 Table	2.093	3.124	0.052	0.479	2.502
2–3 Table	1.050	0.034	3.117	3.284	3.064
1–3 Table	3.143	2.903	2.785	3.2	3.197

pronounced strain concentration occurring in the vicinity of the simulated fault zones. Such localized concentration of deformation demand near fault crossings is consistent with observations reported in previous studies on fault-affected underground structures (Bray and Travasarou, 2007; Karamitros et al., 2007).

For ground-motion cases dominated by a single fault rupture, the peak strain demand is primarily concentrated near the corresponding

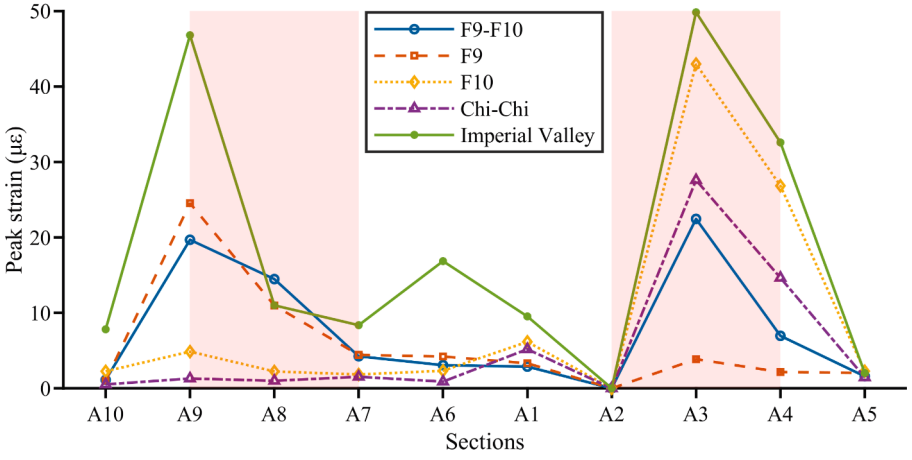

(a) Variation of circumferential strain at the left springing along the tunnel axis

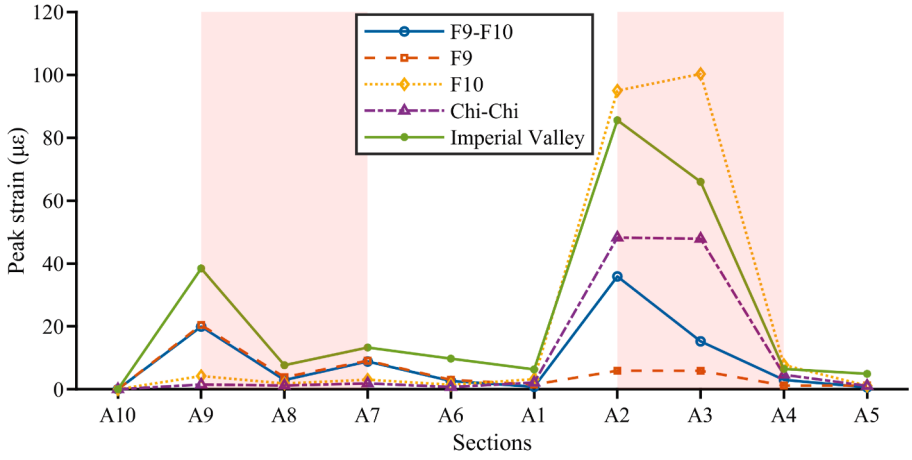

(b) Variation of circumferential strain at the right arch foot along the tunnel axis

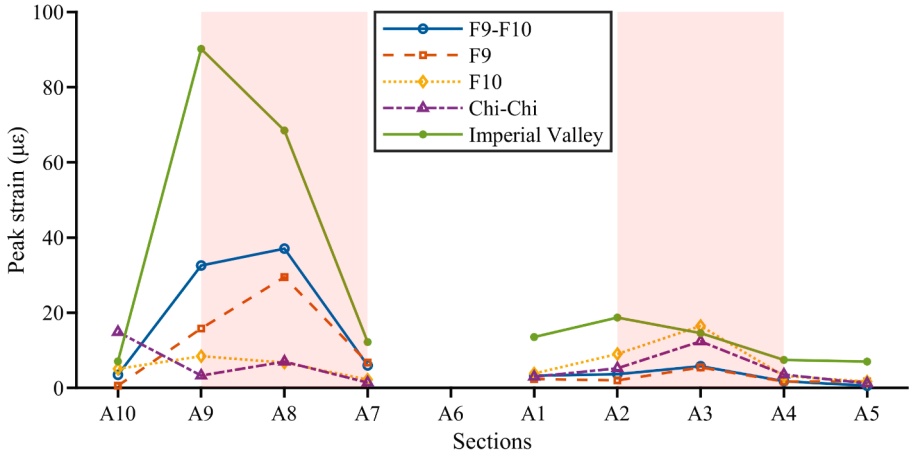

(c) Change in strain along the tunnel axis towards the left spandrel

Fig. 5. Variation of maximum strain along the tunnel length direction at the same detection location on different monitoring sections of tunnel lining.

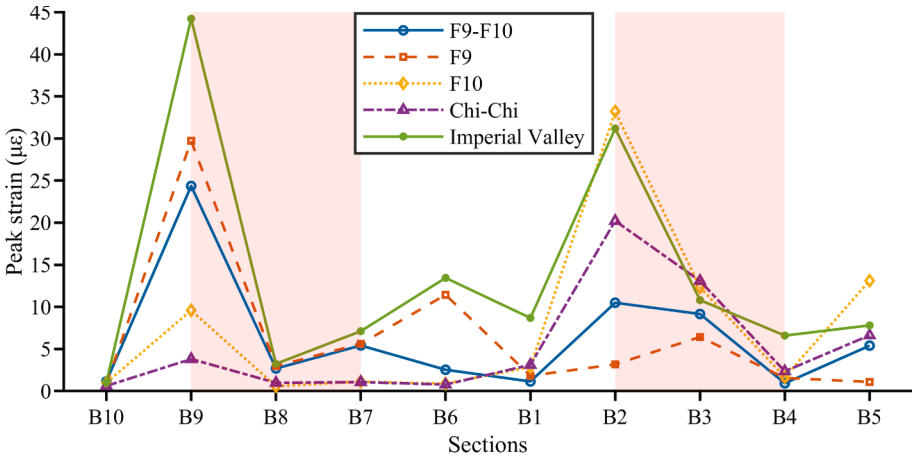

(d) Variation of axial strain of inverted arch along the tunnel axis

Fig. 5. (*continued*).

fault interface, while strain levels away from the fault zone decrease rapidly along the tunnel axis. This spatial pattern indicates that tunnel response is governed by localized deformation induced by fault-crossing relative motion rather than by uniform shaking along the tunnel length.

In contrast, for cases involving simultaneous rupture of both faults or across-fault recorded ground motions, elevated strain demand is observed near both fault interfaces. The presence of multiple strain concentration zones reflects the superposition of relative motion effects across multiple fault crossings, resulting in a more complex spatial response pattern along the tunnel lining.

Comparison between the conventional lining and the seismic-mitigation lining shows that, although the overall spatial distribution pattern of strain remains similar, the peak strain values near fault interfaces are generally reduced in the mitigation configuration. This observation suggests that the mitigation measures primarily influence the magnitude of localized deformation demand, while the spatial locations of strain concentration are controlled by fault-induced relative motion.

4.2. Limitations of absolute-motion-based intensity measures

This section first considers a comprehensive set of ground-motion intensity measures (IMs) as possible. By comparing, across different input-motion cases, the consistency between the amplitude rankings of IMs and those of the measured lining strain responses, the capability of different IMs to reflect the seismic response of fault-crossing structures is examined.

IMs are key parameters for quantifying ground-motion severity and provide a comparable and practical basis for seismic analysis and design. In this study, the applicability of different IMs is examined through subsequent ranking comparisons and correlation analyses between input motions and structural responses. Four categories of IMs—acceleration-based, velocity-based, displacement-based, and composite measures—are considered, as listed in Table 6. In addition, in view of the characteristic damage mechanisms of fault-crossing underground structures, three composite IMs (Nos. 16, 18, 19) are proposed and included for further examination.

In Table 6, $u(t)$ denotes the displacement time history, and t_f denotes the total duration of the ground-motion. $S_a(T)$, $S_v(T)$, and $S_d(T)$ represent the 5 %-damped acceleration, velocity, and displacement response spectra at period T, respectively.

4.2.1. Ranking performance of absolute-motion-based intensity measures

Based on the intensity measures defined in Table 6, the ranking performance of absolute-motion-based intensity measures is first examined. For each input-motion case, the values of individual absolute IMs are calculated from the ground-motion record at a single location and ranked according to their magnitude. The resulting ordering is then compared with the ranking of the measured peak lining strain responses

Table 6
Ground-motion intensity measures.

Number	Type	Intensity Measures	Formula
1	Acceleration type	Peak Ground Acceleration	$PGA = \max\lvert\ddot{u}(t)\rvert$
2		Squared Drift(Nau and Hall, 1984)	$A_{sq} = \int_0^{t_f} \ddot{u}^2(t)dt$
3		Arias Intensity(Arias, 1970)	$I_A = \frac{\pi}{2g}\int_0^{t_f} \ddot{u}^2(t)dt$
4		Average Acceleration Spectrum(Xu et al., 2022)	$S_{a,ave} = \frac{\int_0^5 S_a(T)dT}{5}$
5	Velocity type	Peak Ground Velocity	$PGV = \max\lvert\dot{u}(t)\rvert$
6		Effective Velocity(Trifunac and Brady, 1975)	$V_e = \sqrt{\frac{1}{T}\int_0^{t_f} \dot{u}(t)^2 dt}$
7		Cumulative Absolute Velocity (Mackie, 2004)	$CAV = \int_0^{t_f} \lvert\dot{u}(t)\rvert dt$
8		Squared Velocity(Nau and Hall, 1984)	$V_{sq} = \int_0^{t_f} \dot{u}^2(t)dt$
9		Velocity Intensity(Mackie, 2004)	$I_v = \frac{1}{PGV}\int_0^{t_f} \dot{u}^2(t)dt$
10		Average Velocity Spectrum(Xu et al., 2022)	$S_{v,ave} = \frac{\int_0^5 S_v(T)dT}{5}$
11	Displacement type	Peak ground Displacement	$PGD = \max\lvert u(t)\rvert$
12		Cumulative Absolute Displacement(Mackie, 2004)	$CAD = \int_0^{t_f} \lvert u(t)\rvert dt$
13		Effective Displacement	$D_e = \sqrt{\frac{1}{T}\int_0^{t_f} u(t)^2 dt}$
14		Drift Intensity(Mackie, 2004)	$I_D = \frac{1}{PGD}\int_0^{t_f} u^2(t)dt$
15		Average Drift Spectrum(Xu et al., 2022)	$S_{d,ave} = \frac{\int_0^5 S_d(T)dT}{5}$
16	Combination type	Ratio of PGD to PGV	PGD/PGV
17		Ratio of PGD to PGA (Gehl et al., 2013)	PGD/PGA
18		Ratio of CAD to CAV	CAD/CAV
19		Ratio of D_e to V_e	D_e/V_e
20		Hadiani Intensity(Hadiani et al., 2013)	$I_{VA} = \sqrt{PGV \cdot A_{sq}}$

obtained from the shaking table tests.

For the ranking analysis, lining strain responses at selected locations were considered. Since fault-induced deformation mainly affects the transverse response of the tunnel, strain measurements at the crown and invert were not included in the ranking comparison. Instead, responses at the shoulder, haunch, and springline, which are more sensitive to fault-crossing deformation, were used.

Accordingly, the monitoring sections A7, A8, and A9 located in the vicinity of Fault F9 were selected for analysis, together with three seismic hazard levels corresponding to frequent, rare, and extremely rare earthquakes.

Fig. 6 illustrates representative comparisons between the rankings of absolute-motion-based IMs and the corresponding rankings of peak lining strain demand across different ground-motion cases. From a ranking-consistency perspective, an IM is considered to perform satisfactorily if its relative magnitude ordering agrees with that of the observed structural response.

Here, the percentage of cases with full ranking consistency is defined as the proportion of comparison cases in which the ranking order of a given IM is exactly the same as that of the measured peak lining strain responses. A value of 0 % indicates that no examined case achieved complete ranking agreement, rather than missing data or zero structural response.

The results show that most absolute-motion-based IMs exhibit poor ranking consistency with the measured lining strain demand. Ground motions producing relatively large values of peak acceleration, velocity, or displacement at a single location do not necessarily correspond to higher strain responses in the tunnel lining. Conversely, some ground motions associated with lower absolute IM values induce more severe lining deformation.

This inconsistency is observed across different types of absolute IMs, including acceleration-based, velocity-based, and displacement-based measures. The inability of these IMs to reproduce the observed response ordering indicates that single-point absolute ground-motion is inadequate to capture the dominant factors governing the seismic response of fault-crossing tunnels.

4.2.2. *Ranking performance of relative-motion-based intensity measures*

Following the observed inconsistency of absolute-motion-based intensity measures in reproducing the response ranking of fault-crossing tunnels, it is necessary to examine whether intensity measures incorporating fault-induced relative motion can better reflect the severity ordering of structural response. This subsection focuses on the ranking performance of relative-motion-based IMs defined in Table 6, while maintaining the same ranking-consistency criterion adopted for absolute-motion-based measures. In this analysis, relative-motion-based IMs are derived from the displacement and velocity differences across the identified fault interface. For each ground-motion case, the values of these IMs are calculated and ranked according to their magnitude, and the resulting ordering is compared with the ranking of the measured peak lining strain responses obtained from the shaking table tests. An IM is considered to perform well in a ranking sense if the ordering of its values is consistent with the observed ordering of lining strain demand.

Fig. 7 shows that the introduction of relative motion substantially improves the ranking performance compared with absolute-motion-based measures. However, the effectiveness varies among different relative-motion-based intensity measures. The highest level of ranking consistency is achieved by ratio-type relative IMs, such as the ratio between peak relative displacement and peak relative velocity (PGD/PGV), indicating their superior ability to reproduce the severity ordering of tunnel lining strain demand.

Relative-motion-based intensity measures that primarily characterize the amplitude of fault-crossing relative displacement, such as *CAD* and D_e, also demonstrate improved ranking consistency compared with absolute-motion-based IMs, but their performance is more moderate. This suggests that while these measures effectively capture the overall intensity of relative deformation, they are less sensitive to differences in the temporal characteristics of relative motion.

Other relative-motion-based IMs exhibit limited ranking consistency, indicating that the inclusion of relative motion is a necessary but not sufficient condition for reliable response ranking. The results highlight that relative-motion-based IMs must be carefully formulated to directly reflect both the dominant deformation scale and the associated motion characteristics governing the seismic response of fault-crossing tunnels.

To further quantify the ranking consistency between the candidate IMs and the measured tunnel lining strain responses, Kendall's tau coefficient was calculated. Kendall's tau is a non-parametric rank correlation coefficient that evaluates the degree of concordance between two ranking sequences. Its value ranges from − 1 to 1. A positive value indicates that the IM ranking is generally consistent with the response ranking, a value close to zero indicates weak ranking agreement, and a negative value suggests an opposite ranking tendency. In this analysis, all candidate IMs were calculated from relative ground-motion time histories to ensure a consistent comparison basis.

As shown in Table 7, the calculated Kendall's tau values further confirm that the ranking performance varies significantly among different IMs. Several IMs, including PGA, A_{sq}, I_A, $S_{a,ave}$, and $S_{d,ave}$, exhibit negative Kendall's tau values of approximately − 0.241, indicating poor consistency with the measured lining strain ranking. Some IMs show positive ranking consistency to varying degrees. For example, PGD, *CAD/CAV*, and D_e/V_e have Kendall's tau values of 0.226, 0.241, and 0.381, respectively. Among all examined IMs, PGD/PGV achieves the highest Kendall's tau value of 0.471, demonstrating the best capability to preserve the severity ordering of the measured lining strain responses in the present dataset.

4.3. *Correlation analysis between intensity measures and lining strain response*

To quantitatively evaluate the relationship between seismic intensity

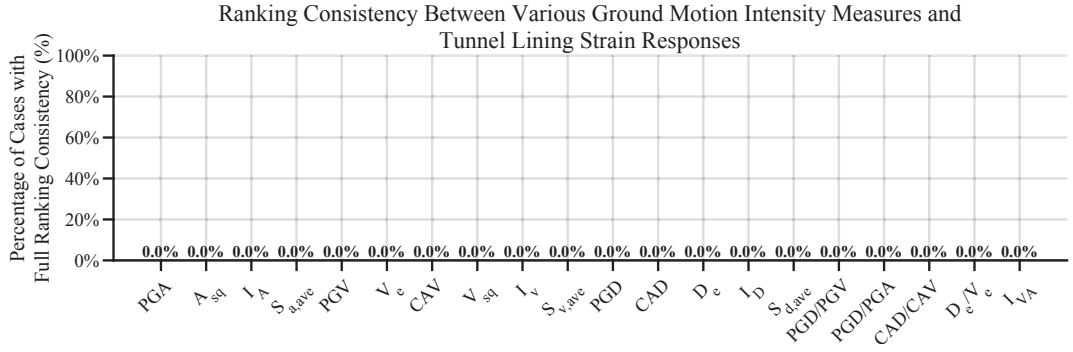

Fig. 6. Comparison results of intensity measures and strain under absolute earthquake ground-motion time history.

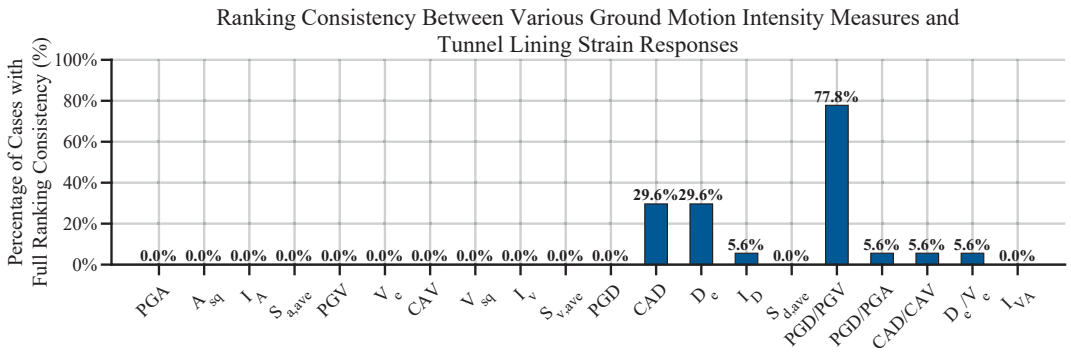

Fig. 7. Comparison results of intensity measures and strain under relative-motion time histories.

Table 7
Kendall's tau coefficients between relative-motion-based IMs and tunnel lining strain responses.

IM	PGA	A_{sq}	I_A	$S_{a,ave}$	PGV	V_e	CAV	V_{sq}	I_v	$S_{v,ave}$
Kendall's tau	−0.241	−0.241	−0.241	−0.241	0.159	−0.041	−0.174	−0.041	−0.174	−0.231
IM	PGD	CAD	D_e	I_D	$S_{d,ave}$	PGD/PGV	PGD/PGA	CAD/CAV	D_e/V_e	I_{VA}
Kendall's tau	0.226	−0.025	−0.225	−0.025	−0.241	0.471	0.041	0.241	0.381	−0.031

measures and tunnel lining strain response, correlation analysis is conducted for selected intensity measures. Prior to regression analysis, logarithmic transformations were applied to both the IM values and the measured peak lining strain responses. This treatment was adopted for two reasons. First, both the considered IMs and the strain responses are positive quantities and may vary over a relatively wide range under different fault-crossing ground-motion inputs. Second, logarithmic transformation can reduce scale effects and alleviate potential heteroscedasticity in regression analysis.

In the following, correlation analyses are performed for different categories of intensity measures under fault-crossing excitation, with consistent preprocessing and evaluation criteria adopted throughout.

4.3.1. Single-IM prediction based on absolute ground-motion time histories

Based on the intensity measures defined in Table 6, correlation analysis is first performed using single absolute-motion-based intensity measures. Representative acceleration-, velocity-, and displacement-based IMs are individually correlated with the measured peak lining

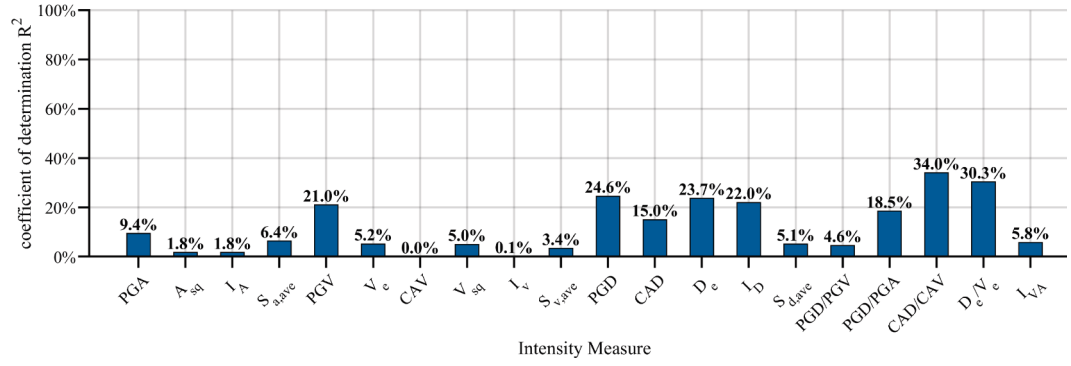

(a)Unmitigated structure

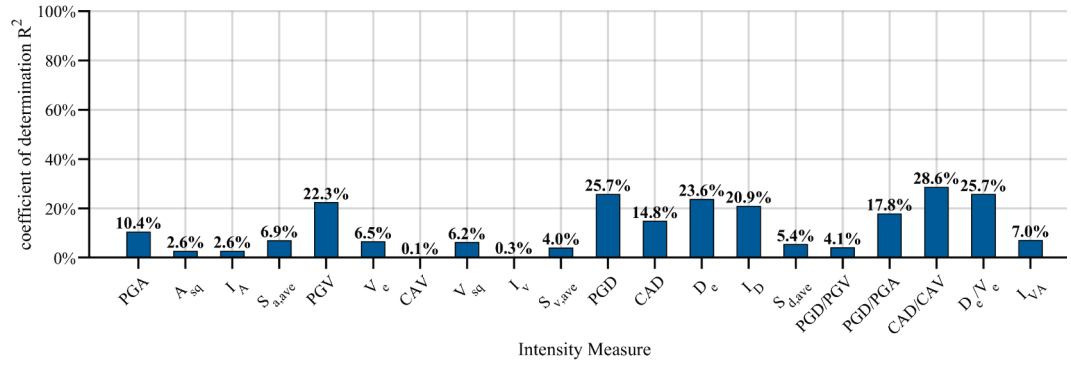

(b)Mitigated structure

Fig. 8. Single-index prediction under absolute ground-motion time histories.

strain responses obtained from the shaking table tests. To examine the influence of seismic mitigation, the analysis is conducted separately for the unmitigated tunnel structure and the mitigated tunnel structure, as illustrated in Fig. 8(a) and Fig. 8(b), respectively.

For the unmitigated structure (Fig. 8(a)), absolute-motion-based IMs exhibit generally low correlation with lining strain demand. Most IMs show coefficient of determination, R^2 below approximately 25 %, with substantial scatter observed across different ground-motion cases. Among the considered measures, PGA and spectral acceleration–based IMs demonstrate limited correlation, while velocity- and displacement-based absolute IMs do not provide consistent improvement. These results indicate that the amplitude of ground-motion recorded at a single location is inadequate to characterize the deformation demand imposed on the unmitigated fault-crossing tunnel.

For the mitigated structure (Fig. 8(b)), a similar trend is observed. Although the application of seismic mitigation alters the overall response level of the tunnel lining, the correlation between single absolute-motion-based IMs and lining strain demand remains weak. Some IMs exhibit slightly higher coefficient of determination, R^2 compared with the unmitigated case; however, the overall correlation levels remain low, and no absolute-motion-based IM demonstrates robust and stable correlation across all ground-motion cases and hazard levels.

Although these two cases provide the best-performing regressions among the absolute-motion-based IMs (Fig. 9), the coefficients of determination remain below 0.35, implying considerable dispersion and demonstrating that IMs derived solely from absolute displacement records are inadequate to reliably explain or predict the strain response of fault-crossing tunnel linings.

The comparison between unmitigated and mitigated structures indicates that seismic mitigation does not fundamentally improve the capability of absolute-motion-based IMs to characterize tunnel lining strain response under fault-crossing excitation. The observed limitations are therefore attributed to the inherent inability of single-point absolute ground-motion intensity to capture fault-induced relative deformation, rather than to the absence or presence of mitigation measures. This observation motivates the subsequent examination of correlation performance using relative-motion-based intensity measures.

4.3.2. *Correlation analysis using single relative-motion-based intensity measures*

Correlation analysis is performed using single relative-motion-based intensity measures to further quantify their ability to characterize tunnel lining strain response. The analysis is conducted separately for the unmitigated and mitigated tunnel structures, and the coefficient of determination R^2 obtained from logarithmically transformed data is used as the evaluation metric. Fig. 10 presents the correlation results, in terms of the coefficient of determination R^2, between single relative-motion-based intensity measures and peak lining strain response for the unmitigated and mitigated tunnel structures, respectively.

For the unmitigated tunnel structure (Fig. 10(a)), relative-motion-based intensity measures exhibit a pronounced improvement in correlation with peak lining strain demand compared with absolute-motion-based IMs. Relative displacement–related measures, such as PGD, *CAD*, and D_e, achieve the highest correlation levels, with R^2 values generally in the range of approximately 30 %–40 %. This indicates that fault-induced relative displacement plays a dominant role in governing the lining deformation response under fault-crossing excitation.

In contrast, certain relative-motion-based IMs exhibit limited correlation performance. Notably, the ratio-type intensity measure PGD/PGV, which demonstrated excellent performance in the ranking-consistency analysis, shows very low R^2 values in the correlation analysis. This behavior reflects the intrinsic characteristics of ratio-type relative intensity measures: their values are insensitive to amplitude scaling of ground-motion records. As a result, although PGD/PGV is effective in distinguishing the relative severity ordering of different ground-motion cases, it does not capture variations in response magnitude required for regression-based correlation analysis.

For the mitigated tunnel structure (Fig. 10(b)), similar trends are observed. Relative displacement–based IMs continue to exhibit the strongest correlation with lining strain response, with R^2 values reaching approximately 40 %–45 %, indicating that relative displacement remains the primary factor controlling deformation demand even when seismic mitigation measures are applied.

As shown in Fig. 11, although the fitting performance is improved compared with the single-IM results based on absolute ground-motion, the coefficients of determination remain below 0.50, suggesting considerable dispersion and indicating that a single intensity measure is still inadequate to capture the coupled effects of fault-induced differential displacement.

As in the unmitigated case, the ratio-type IM PGD/PGV shows weak correlation performance for the mitigated structure. The persistence of this behavior confirms that the observed limitation is associated with the intrinsic properties of ratio-type intensity measures, rather than the presence or absence of mitigation measures.

Overall, the correlation results demonstrate that while single relative-motion-based IMs significantly outperform absolute-motion-based measures, no individual relative-motion-based IM is capable of simultaneously achieving robust ranking consistency and strong correlation with lining strain response. Ratio-type IMs are effective for ranking but inadequate for amplitude-based correlation, whereas displacement-based IMs exhibit improved correlation but limited ability to capture all aspects of response variability. This observation provides a clear motivation for the subsequent development of a multi relative-motion-based intensity measure framework.

To further examine whether the difference in correlation perfor-

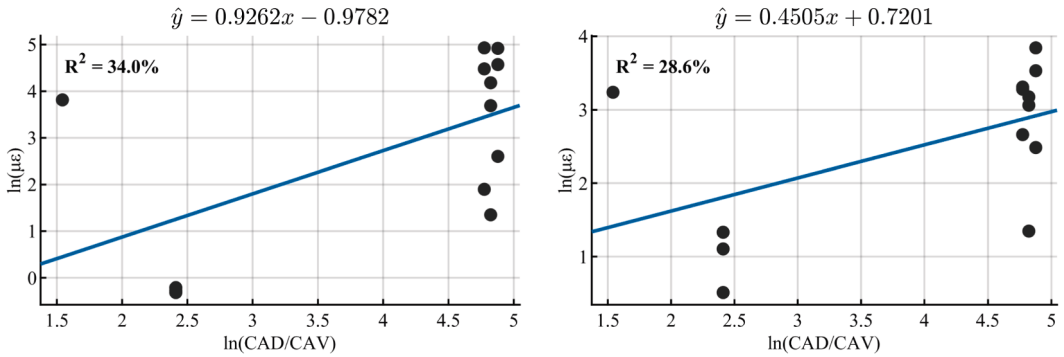

Fig. 9. The best-fit result in Fig. 8.

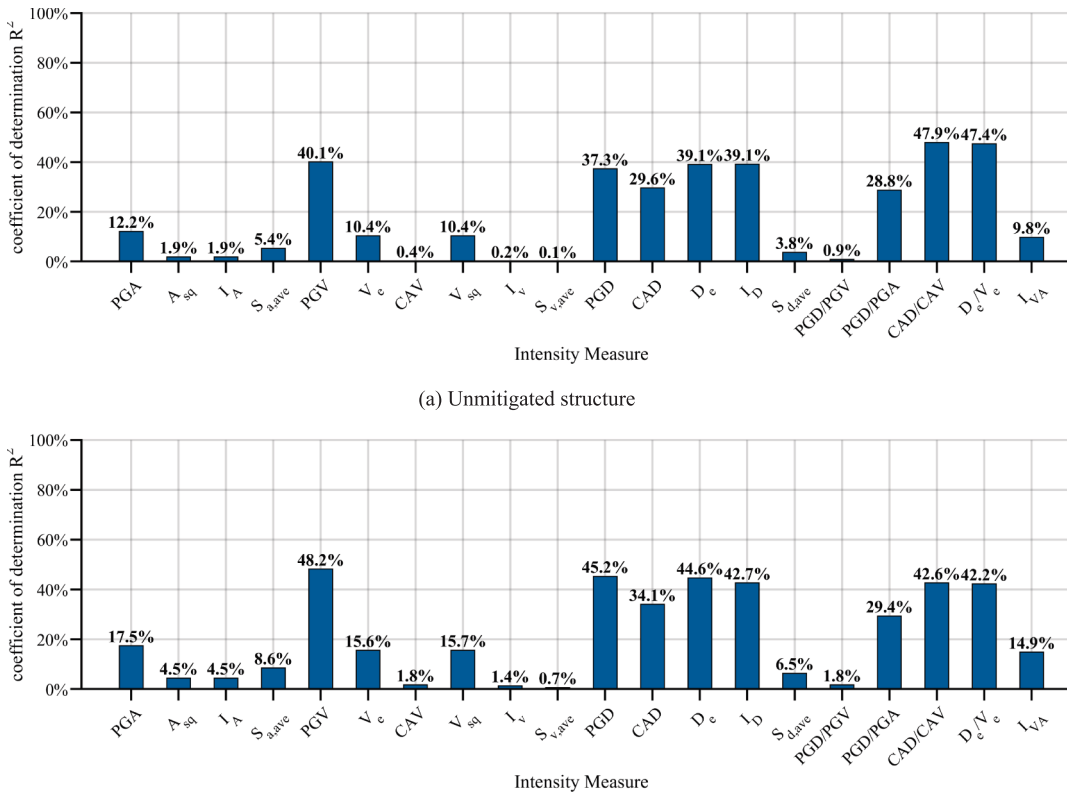

Fig. 10. Single-index prediction under relative earthquake ground-motion time history.

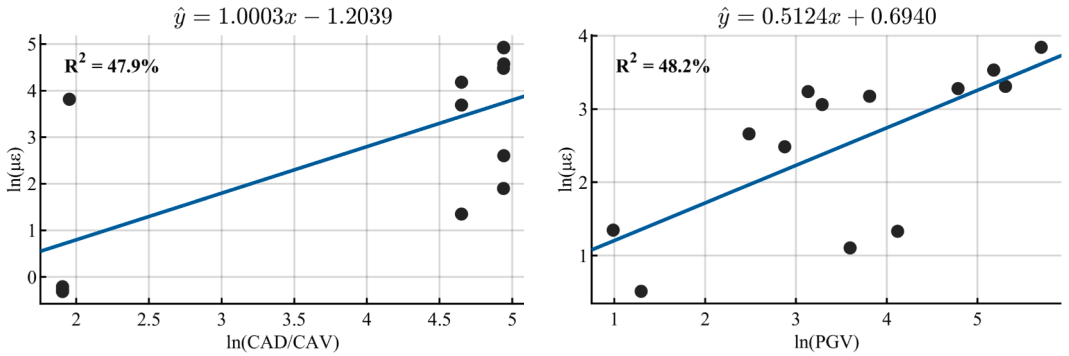

Fig. 11. The best-fit result in Fig. 10.

mance between the unmitigated and mitigated tunnel structures is statistically significant, Fisher's z-transformation was used to compare the IM–response correlation coefficients obtained for the two structural configurations. The analysis was conducted separately for the absolute-motion-based IMs and the relative-motion-based IMs, corresponding to Fig. 8 and Fig. 10, respectively. For each candidate IM, the coefficient of determination R^2 was first converted to the corresponding correlation magnitude using $r = \sqrt{R^2}$, because the fitted IM–response trends considered here were positive. Fisher's z-transformation was then applied to the two correlation coefficients obtained from the unmitigated and mitigated structures. The null hypothesis assumes that, for a given IM, the correlation coefficient between the IM and the measured peak lining strain response is not significantly different between the two structural configurations.

For the absolute-motion-based IMs shown in Fig. 8, none of the examined IMs exhibits a statistically significant difference between the unmitigated and mitigated structures at the 0.05 significance level. The minimum p-value among all absolute-motion-based IMs is 0.6878, which is still much larger than 0.05. Similarly, for the relative-motion-based IMs shown in Fig. 10, all calculated p-values are greater than 0.05, with the minimum p-value being 0.8069. These results indicate that the apparent differences in R^2 values between the two structural configurations are not statistically significant within the present test dataset. Therefore, although the mitigation measures change the response amplitude of the tunnel lining, they do not fundamentally alter the correlation relationship between the selected IMs and the measured strain response. This result further supports the interpretation that the dominant IM–response relationship is mainly governed by fault-induced relative deformation rather than by the presence or absence of

mitigation measures.

4.3.3. Correlation analysis using multi relative-motion-based intensity measures

The preceding analyses demonstrate that single relative-motion-based intensity measures emphasize different aspects of fault-crossing ground-motion and exhibit complementary performance in terms of ranking consistency and correlation with lining strain response. In particular, ratio-type IMs such as PGD/PGV provide robust response ranking but poor amplitude-based correlation, whereas displacement-related relative IMs exhibit improved correlation but limited ability to distinguish response severity ordering. This complementary behavior motivates the development of a multi relative-motion-based intensity measure framework, in which different descriptors of fault-induced deformation are jointly considered.

Based on the results obtained for single-IM analyses, PGD/PGV is selected as a core component of the multi-IM framework. As demonstrated in the preceding sections, PGD/PGV provides the most stable response ranking among all considered IMs, reflecting its effectiveness in distinguishing the relative severity of different fault-crossing ground-motion cases. At the same time, PGD/PGV is inherently insensitive to amplitude scaling of ground-motion records and therefore cannot capture variations in response magnitude. Consequently, PGD/PGV is combined with displacement-related relative IMs that are sensitive to deformation amplitude, including I_D, *CAD*, and D_e, so as to jointly represent both response ordering and magnitude characteristics.

It is noted that multi-absolute-motion-based intensity measures are not further considered. Results from both ranking and correlation analyses have consistently shown that absolute-motion-based IMs are inadequate to capture the dominant fault-induced deformation mechanism governing tunnel response. Since all absolute IMs describe ground-motion intensity at a single location and lack information on relative deformation across the fault interface, combining multiple absolute IMs does not introduce fundamentally new information relevant to the problem considered.

Fig. 12 compares the correlation performance of different multi relative-motion-based intensity measure combinations in terms of the coefficient of determination R^2, with (a) and (b) corresponding to the unmitigated and mitigated tunnel structures, respectively. The results indicate that multi-IM formulations lead to a substantial enhancement in correlation performance compared with single-IM analyses for both structural configurations.

For the unmitigated structure, most multi-relative-IM combinations achieve R^2 values exceeding 70 %, with several combinations reaching values above 80 %. Similar trends are observed for the mitigated structure, where correlation levels are further enhanced and several combinations approach or exceed 90 %. These results demonstrate that jointly considering complementary relative-motion descriptors significantly strengthens the IM–response relationship, regardless of the presence of seismic mitigation measures.

Based on the overall comparison presented in Fig. 12, combinations involving PGD/PGV paired with I_D, *CAD*, and D_e consistently exhibit the highest correlation levels for both unmitigated and mitigated tunnel structures. These combinations are therefore selected for further detailed examination.

Fig. 13 illustrates the three-dimensional correlation surfaces between peak lining strain response and the selected multi relative-motion-based intensity measure combinations, in which PGD/PGV is paired with I_D, *CAD*, D_e, and PGD. Fig. 13(a), (c), (e), (g) correspond to the unmitigated tunnel structure, while Fig. 13(b), (d), (f), (h) correspond to the mitigated structure. For the multi-IM regression analysis, a second-order polynomial surface was adopted to fit the relationship between the logarithmically transformed peak lining strain response and the selected pairs of relative-motion-based Ims.

For both structural configurations, the fitted response surfaces exhibit smooth and monotonic trends, indicating a stable relationship

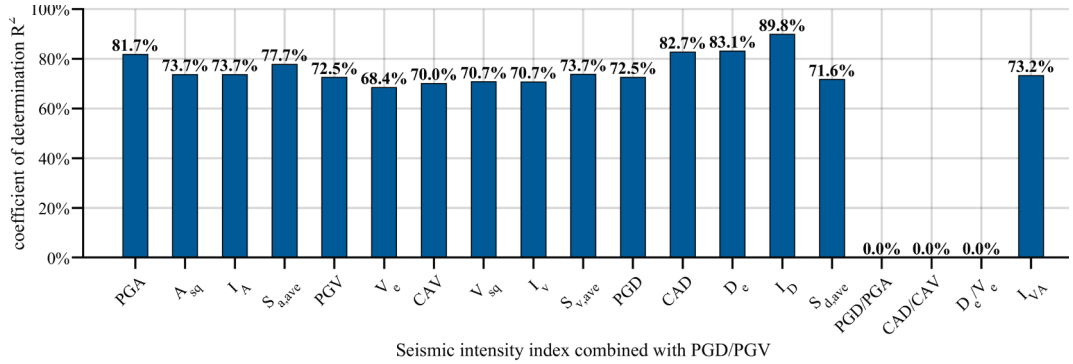

(a)Unmitigated structure

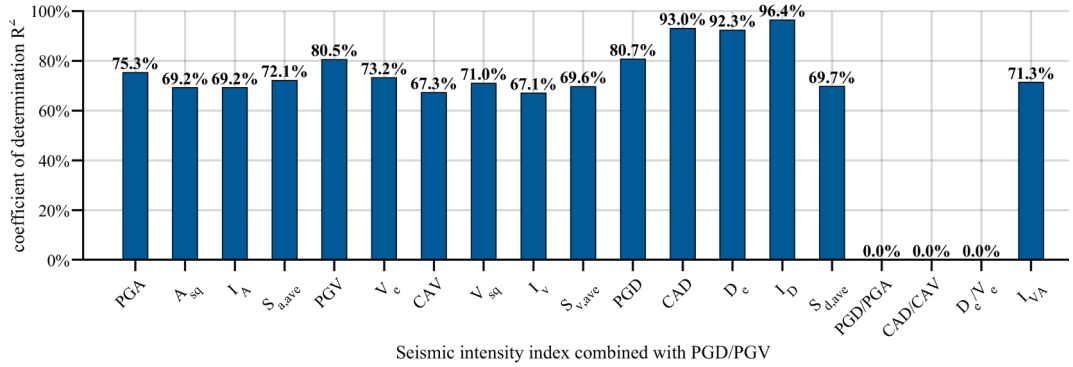

(b)Mitigated structure

Fig. 12. Multi-IM prediction based on relative ground-motion time histories.

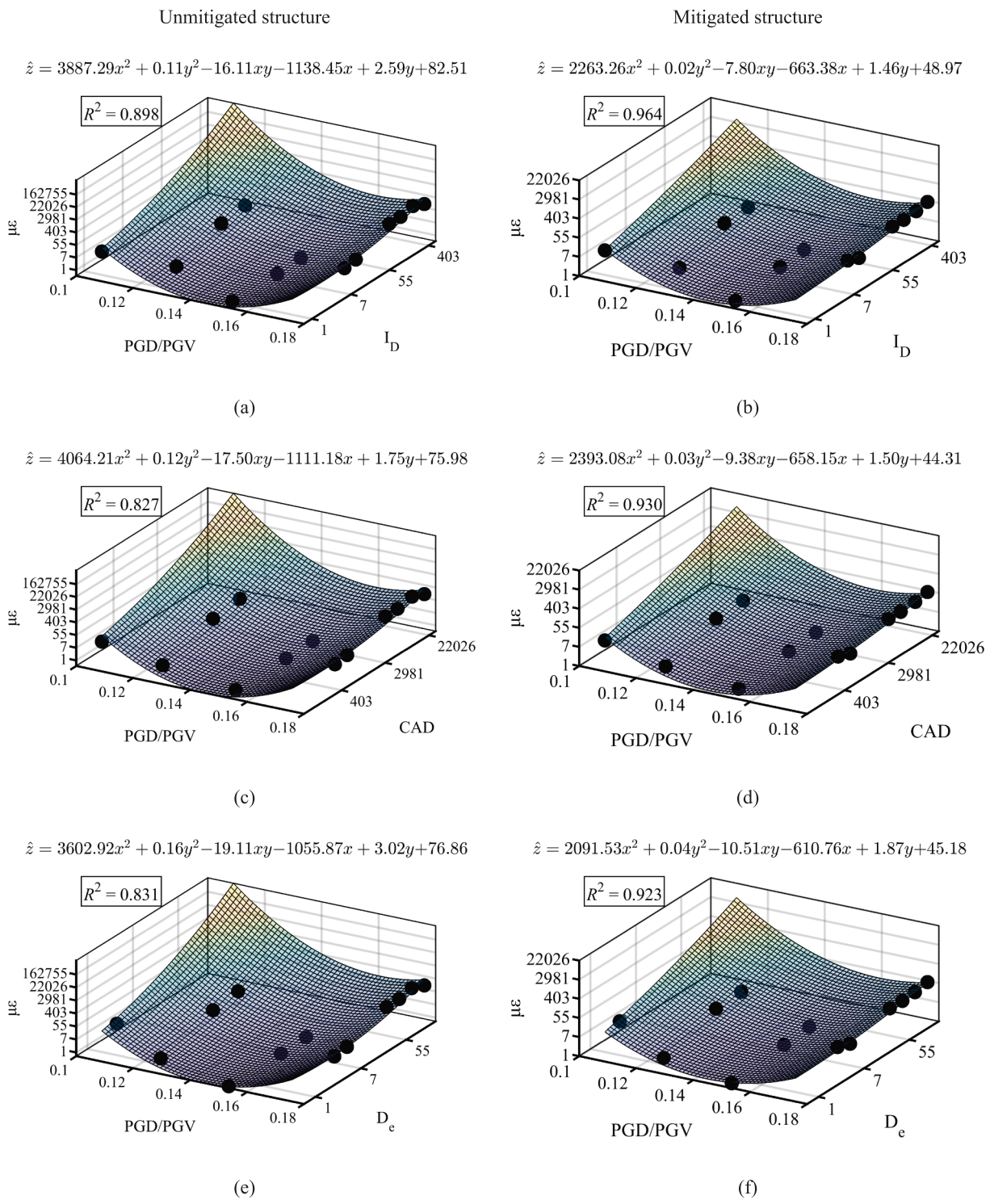

Fig. 13. Fitting of multiple Intensity Measures and structural responses.

between the combined intensity measures and lining strain demand. The overall patterns observed for the mitigated structure are consistent with those of the unmitigated structure, despite differences in response magnitude due to seismic mitigation. These results suggest that the selected multi-relative-IM combinations provide a consistent description of the IM–response relationship across different structural conditions.

It should be noted that the PGD/PGV–PGD combination does not outperform the PGD/PGV–I_D, PGD/PGV–CAD, and PGD/PGV–D_e combinations in terms of fitting accuracy. Nevertheless, this combination has better practical applicability because both PGD/PGV and PGD can be directly derived from displacement and velocity time histories, which are commonly available in ground-motion records and numerical simulations. In contrast, I_D, *CAD*, and D_e require additional calculation procedures and may not be routinely considered in standard ground-motion selection. Therefore, the PGD/PGV–PGD combination can be regarded as a more convenient but slightly less accurate alternative for engineering implementation.

Although the present study focuses on a perpendicular fault-crossing

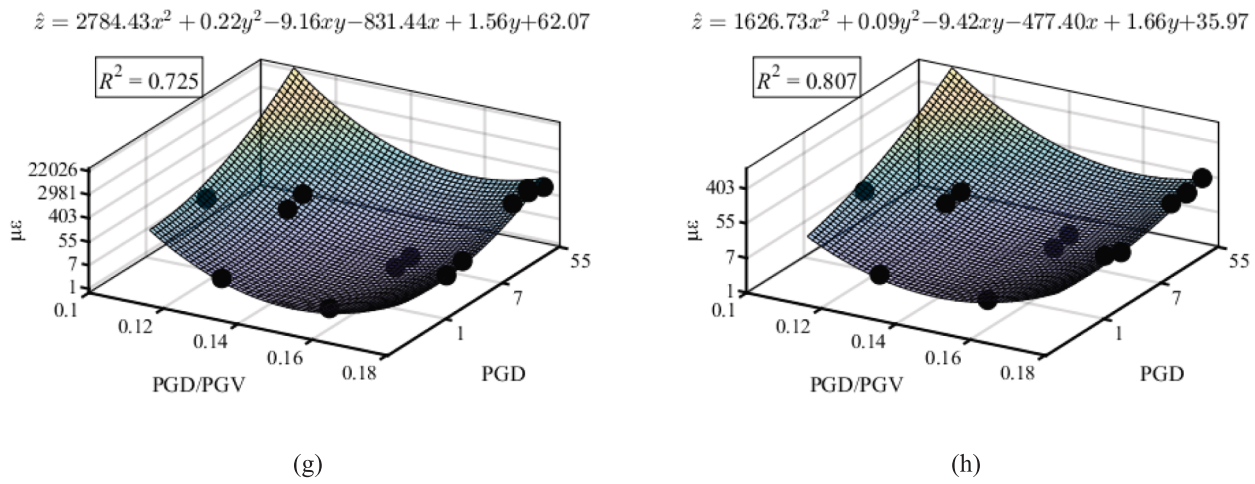

Fig. 13. (*continued*).

tunnel, the proposed IM framework is not inherently limited to this configuration. The controlling mechanism of the selected IMs is the relative movement between the two sides of the fault, rather than the geometric intersection angle itself. When the tunnel crosses the fault obliquely, the fault-induced relative displacement and velocity can be projected onto the local longitudinal, transverse, and vertical directions of the tunnel. In this case, the same relative-motion-based IMs can still be used to characterize the deformation demand acting on the tunnel. Therefore, the intersection angle is not expected to change the basic applicability of the proposed IMs. However, it may change the dominant response component and the fitted coefficients of the IM–response relationship. Further validation using oblique fault-crossing configurations is still needed to quantify this influence.

To further examine whether the fitted relationships are statistically reasonable, residual analysis was conducted for the selected multi-IM regression models. The residual was defined as the difference between the logarithmically transformed measured strain response and the corresponding fitted value. The standardized residuals were then plotted against the fitted values to examine whether the residuals were randomly distributed around zero and whether obvious heteroscedasticity or systematic bias existed.

As shown in Fig. 14, the standardized residuals are generally distributed around zero without an obvious trend with the fitted values. No clear funnel-shaped pattern is observed, suggesting that the fitted models do not exhibit evident heteroscedasticity. Most standardized residuals are located within the range of − 2 to 2, indicating that no severe outliers are present. In addition, the normal Q–Q plots show that the residual points are mostly distributed along the reference line, suggesting that the residuals approximately follow a normal distribution. Although slight tail deviations are observed for some models, these deviations are acceptable considering the limited number of experimental data points. Therefore, the residual diagnostics support the statistical reasonableness of the logarithmically transformed regression models within the scope of the present test data.

To further examine the predictive capability of the fitted multi-IM models and reduce the potential concern of overfitting, an independent validation analysis was conducted. In the multi-IM regression analysis, the second-order polynomial surfaces shown in Fig. 13(a)–(h) were fitted using the strain response data and corresponding IM values from the frequent, rare, and extremely rare earthquake levels. The data from the moderate earthquake level were not used in the fitting process and were reserved as an independent validation dataset.

The eight fitted models, corresponding to four IM combinations for the unmitigated and mitigated tunnel structures, were then used to predict the peak lining strain responses under the moderate earthquake cases. The predicted strain responses were compared with the measured values, and the validation performance was evaluated using the coefficient of determination R^2, root-mean-square error (RMSE), and mean absolute error (MAE). This validation procedure provides an additional assessment of whether the fitted surfaces can retain predictive capability for data that were not involved in model calibration. The independent validation results are summarized in Table 8.

As shown in Table 8, the independent validation results indicate that the fitted multi-IM models retain reasonable predictive capability for the moderate earthquake cases that were not used for model calibration. In this validation, R^2 was used to evaluate the ability of the fitted models to explain the variation of the measured strain response, whereas RMSE and MAE were used to quantify the prediction errors. A higher R^2 indicates better agreement between the predicted and measured strain responses, while lower RMSE and MAE values indicate smaller prediction errors. It should be noted that RMSE and MAE were calculated in the same scale as the regression output.

For the unmitigated structure, the PGD/PGV–I_D model provides the best validation performance among the four IM combinations, with the highest R^2 value of 0.7476 and the lowest RMSE and MAE values of 0.8974 and 0.7476, respectively. The PGD/PGV–*CAD* and PGD/PGV–D_e models also show acceptable validation performance, with R^2 values of 0.6981 and 0.6493, respectively. Their RMSE and MAE values are slightly larger than those of PGD/PGV–I_D, indicating a moderate increase in prediction error. In contrast, the PGD/PGV–PGD model gives the lowest R^2 value of 0.6195 and the largest RMSE and MAE values among the four combinations, suggesting relatively weaker prediction accuracy.

For the mitigated structure, a similar trend can be observed. The PGD/PGV–I_D model again achieves the best validation performance, with the highest R^2 value of 0.7779 and the lowest RMSE and MAE values of 0.6249 and 0.5856, respectively. The PGD/PGV–*CAD* and PGD/PGV–D_e models maintain relatively stable predictive capability, with R^2 values of 0.7127 and 0.6776, respectively. Their RMSE and MAE values are also close to those of the PGD/PGV–I_D model, indicating that these two combinations can still provide reasonable prediction accuracy. The PGD/PGV–PGD model shows the lowest validation performance for the mitigated structure, with an R^2 value of 0.5440 and the largest RMSE and MAE values, indicating that its predictive accuracy is relatively limited.

After back-transformation to the original microstrain scale, the fitted models still show moderate to strong correlation with the measured strain responses. The original-scale squared correlation coefficients are 0.647, 0.596, 0.578, and 0.491 for the mitigated structure, and 0.853, 0.726, 0.721, and 0.439 for the unmitigated structure. This indicates that the logarithmic-domain regression does not merely improve the apparent fitting performance in the transformed scale, but also preserves

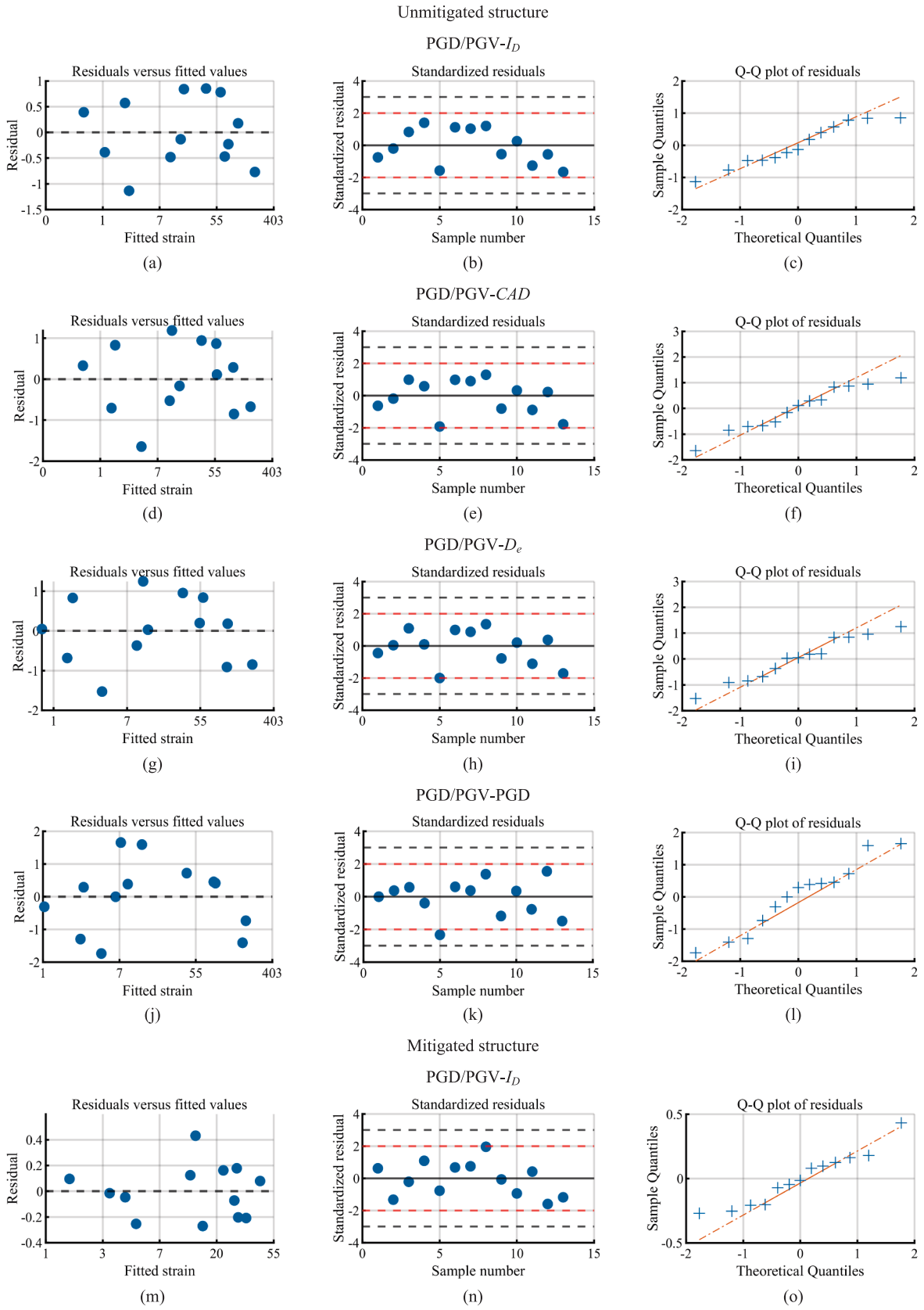

Fig. 14. Residual diagnostics of the selected multi-IM regression models: standardized residuals versus fitted values and normal Q–Q plots.

meaningful predictive consistency in the original strain scale.

Overall, the validation results are consistent with the fitting results shown in Fig. 13. Among the examined IM combinations, PGD/PGV–I_D provides the best overall performance in terms of both explanatory

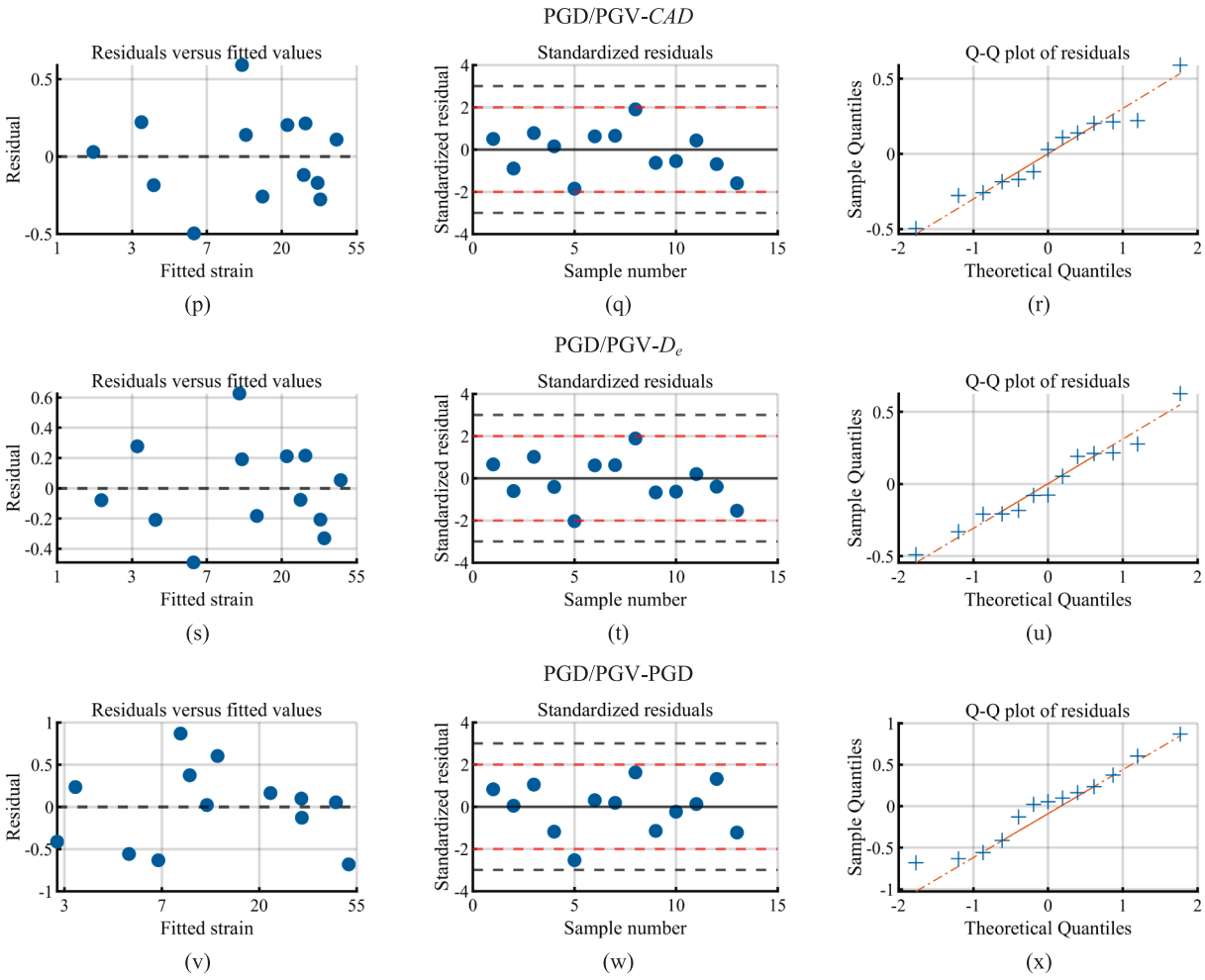

Fig. 14. (*continued*).

Table 8
Independent validation results of the fitted multi-IM models under moderate earthquake cases.

	PGD/PGV-I_D	PGD/PGV-CAD	PGD/PGV-D_e	PGD/PGV-PGD
Unmitigated structure				
R^2	0.7476	0.6981	0.6493	0.6195
RMSE	0.8974	0.9814	1.0578	1.1019
MAE	0.7476	0.8083	0.8747	0.9522
Mitigated structure				
R^2	0.7779	0.7127	0.6776	0.5440
RMSE	0.6249	0.7107	0.7529	0.8954
MAE	0.5856	0.6862	0.7291	0.8801

capability and prediction error. PGD/PGV–*CAD* and PGD/PGV–D_e also show reasonable validation performance, confirming that displacement-related relative IMs can effectively complement PGD/PGV in characterizing tunnel lining strain response. Although the PGD/PGV–PGD combination exhibits lower prediction accuracy, it still has practical value because PGD is more readily obtainable in engineering applications. These results indicate that the improved performance of the multi relative-motion-based IM framework is not solely caused by in-sample fitting, but is also supported by its predictive capability for the moderate earthquake cases that were not included in the regression calibration. Nevertheless, because the validation data were still obtained from the same shaking table test program, the results should be interpreted as internal validation evidence within the present experimental conditions rather than proof of universal applicability.

5. Discussion on the selection of intensity measures for fault-crossing tunnels

5.1. Interpretation of intensity-measure performance

The results demonstrate that no single intensity measure can simultaneously achieve stable response ranking and strong correlation with tunnel lining strain demand under fault-crossing seismic excitation. This limitation reflects the multidimensional nature of fault-induced deformation, which cannot be adequately represented by a single descriptor of ground-motion.

Absolute-motion-based intensity measures consistently exhibit poor ranking consistency and weak correlation for both unmitigated and mitigated tunnel structures, indicating that inertial demand alone is inadequate to characterize fault-crossing tunnel response. In contrast, relative-motion-based intensity measures introduce essential information associated with fault-induced deformation and therefore exhibit improved performance. However, distinct trade-offs are observed among different relative IMs: ratio-type measures such as PGD/PGV provide stable response ranking but are insensitive to amplitude scaling, whereas displacement-related relative IMs capture response magnitude more effectively but offer limited capability in distinguishing response severity ordering. These observations indicate that the performance of different intensity measures is governed by the physical characteristics they represent, rather than by statistical form alone.

The different performances of ratio-type and displacement-type relative IMs can be explained from their physical meanings. PGD/PGV

is a ratio between the peak relative displacement and the peak relative velocity. It reflects the deformation characteristic of the relative motion rather than its absolute amplitude. A relatively large PGD/PGV value indicates that the input motion contains a stronger permanent or quasi-permanent displacement component, whereas a smaller value implies that transient vibration is more dominant. Therefore, PGD/PGV is more suitable for distinguishing different fault-crossing deformation mechanisms and preserving the severity ordering of tunnel responses. However, because PGD/PGV is a normalized ratio, it is relatively insensitive to amplitude scaling and cannot directly quantify the absolute level of deformation demand. This explains why it performs well in ranking analysis but shows limited correlation with the magnitude of peak lining strain.

In contrast, displacement-type relative IMs, such as PGD, *CAD*, and D_e, directly describe the amplitude, cumulative effect, or effective level of relative displacement across the fault interface. Since the seismic response of a fault-crossing tunnel is primarily deformation-controlled, these IMs are more directly related to the strain demand of the tunnel lining and therefore show stronger correlation with peak lining strain response. Nevertheless, displacement-type IMs mainly quantify the intensity level of relative deformation and may not fully distinguish whether the response is governed by permanent fault offset or transient vibration. As a result, their ranking consistency may be weaker than that of PGD/PGV when different ground-motion cases have similar displacement amplitudes but different deformation characteristics.

Accordingly, the combination of PGD/PGV and displacement-related relative IMs is physically meaningful because it simultaneously accounts for the deformation mechanism and the deformation intensity of fault-crossing ground motions.

A comparison with existing IM evaluation studies further highlights the particularity of fault-crossing tunnel response. For conventional underground structures or shield tunnels subjected to spatially uniform or site-response-dominated ground shaking, previous studies have reported that acceleration-, velocity-, or spectrum-related IMs may show good predictive performance. For example, PGA, SMA, VSI, or spectral-shape-based IMs have been identified as efficient IMs in some studies on subway stations, rectangular tunnels, or shield tunnels in liquefiable and non-liquefiable soils. These findings are mainly associated with soil–structure interaction, site response, and deformation demand under conventional seismic excitation.

In contrast, the present results show that absolute-motion-based IMs are inadequate for fault-crossing tunnels because they do not contain information on differential movement across the fault. In the present tests, the coefficients of determination of absolute-motion-based IMs are generally lower than 0.35, whereas single relative displacement-related IMs increase the R^2 values to approximately 0.30–0.45. More importantly, the multi-relative-motion-based IM combinations, such as PGD/PGV–ID, PGD/PGV–*CAD*, and PGD/PGV–D_e, generally achieve R^2 values greater than 0.70, with some cases approaching or exceeding 0.90. This improvement indicates that the proposed dual-IM framework provides a more effective description of the fault-crossing demand mechanism by combining a mechanism-oriented descriptor and an amplitude-oriented descriptor.

Nevertheless, the comparison should be interpreted within the differences in structural type, ground-motion input, response quantity, and evaluation method among different studies. The present results do not imply that the proposed IMs are universally superior for all underground structures. Rather, they indicate that relative-motion-based IMs are more appropriate for fault-crossing tunnel problems, where the structural response is primarily governed by fault-induced differential deformation.

5.2. Necessity of a multi relative-motion-based IM framework

The complementary behavior observed among single relative-motion-based intensity measures provides a clear rationale for adopting a multi-IM framework. Fault-crossing tunnel response is governed by both the scale of relative deformation and the manner in which this deformation develops and accumulates during seismic loading. Capturing these characteristics simultaneously requires the joint consideration of multiple descriptors.

In this study, PGD/PGV serves as a ranking-oriented descriptor that effectively distinguishes the relative severity of different ground-motion cases, while displacement-related relative IMs (I_D, *CAD*, and D_e) capture amplitude-dependent deformation demand and cumulative displacement effects. Their combined use overcomes the intrinsic limitations of single-IM formulations and provides a more robust characterization of tunnel lining strain response. The consistent performance of the proposed multi-relative-IM framework for both unmitigated and mitigated tunnel structures further indicates that seismic mitigation modifies response levels but does not alter the fundamental deformation mechanisms governed by fault-induced relative motion.

5.3. Implications for ground-motion selection in fault-crossing design

The proposed multi relative-motion-based IM framework can be further used to guide ground-motion selection for fault-crossing tunnel analysis. Different from conventional record selection procedures that mainly match absolute ground-motion intensity at a single station, the selection of fault-crossing ground motions should simultaneously consider two aspects: the deformation mechanism of the input motion and the intensity level of fault-induced relative displacement. In the proposed framework, PGD/PGV is used as a mechanism-oriented descriptor, whereas displacement-related relative IMs, such as I_D, *CAD*, and D_e, are used as amplitude-oriented descriptors. Therefore, ground-motion selection can be performed in a two-step manner: first identifying the dominant deformation mechanism using PGD/PGV, and then selecting records with appropriate relative-displacement intensity levels using displacement-based IMs.

For a candidate across-fault ground-motion pair, the relative displacement time history should first be obtained by subtracting the displacement histories on the two sides of the fault interface. The corresponding relative velocity history can be calculated by differentiating the relative displacement history. The relative PGD, PGV, I_D, *CAD*, and D_e are then calculated from the relative-motion time histories.

As shown in Table 9, PGD/PGV reflects the relative contribution of peak relative displacement and peak relative velocity and can therefore be used as a mechanism-oriented descriptor for candidate fault-crossing ground motions. In the present dataset, a transition around PGD/PGV = 0.146 was observed. Motions with relatively smaller PGD/PGV values tend to exhibit stronger transient vibration characteristics, whereas motions with relatively larger PGD/PGV values tend to contain more pronounced quasi-permanent or long-period relative displacement components. Therefore, this value is used only as a dataset-specific empirical reference for interpreting the deformation characteristics of the input motions considered in this study. It should not be regarded as a statistically established or universally applicable threshold. For other fault-crossing scenarios, tunnel configurations, fault geometries, or input-motion datasets, the transition range of PGD/PGV should be recalibrated using additional experimental, numerical, or field data.

After the deformation mechanism is identified, displacement-related relative IMs should be used to control the intensity level of selected ground motions. For a given seismic hazard level or design scenario, the selected records should have relative I_D, *CAD*, or D_e values close to the target intensity level. Among these measures, *CAD* and D_e are

Table 9
PGD/PGV of different earthquakes.

PGD/PGV	F9	F10	F9-F10	Chi-Chi	Imperial Valley
F9 fault	0.176	0.128	0.174	0.154	0.109
F10 fault	0.163	0.148	0.146	0.242	0.084

particularly useful because they reflect not only the peak relative displacement but also the cumulative or effective deformation demand during the entire excitation process. In this way, PGD/PGV controls the type of fault-crossing excitation, while displacement-based relative IMs control the severity of the excitation.

5.4. Applicability and limitations of the proposed dual-IM framework

The proposed dual-IM framework was developed and evaluated using fault-crossing tunnel models in the present shaking table test. Therefore, the specific regression coefficients, ranking results, recommended IM combinations, and empirical threshold values should be interpreted within the scope of the tested tunnel configuration, input ground motions, fault geometry, and response indicator adopted in this study. The framework should be regarded as a relative-motion-based evaluation concept rather than a universal empirical formula for all fault-crossing tunnel conditions.

The physical basis of the proposed framework is the relative movement between the two sides of a fault, which represents a key deformation demand for engineering structures crossing active faults. In this sense, the concept is not inherently restricted to tunnels. Other fault-crossing structures, such as underground pipelines, utility tunnels, buried box structures, and bridge foundations crossing fault zones, may also be influenced by relative displacement and velocity demands across the fault interface. However, different structural systems may exhibit distinct stiffness characteristics, boundary conditions, deformation mechanisms, and dominant damage indicators. Therefore, the IM–response relationship and the corresponding regression coefficients should be recalibrated using structure-specific numerical simulations, physical model tests, or field observations before the proposed framework is applied to other types of structures.

It should also be noted that the effects of tunnel burial depth and surrounding-medium conditions were not explicitly investigated in the present study. In the shaking table tests, the ground motions were directly prescribed through the shaking tables, and the evaluated IMs were calculated from the input motions of individual tables or from the relative motions between adjacent tables. Therefore, tunnel burial depth and surrounding-medium conditions were not independent variables in the IM calculation, and they are not expected to directly change the relative comparison of different IMs within the present experimental setup. However, this does not mean that tunnel depth and surrounding-medium properties are negligible in prototype engineering applications. In real sites, burial depth and soil or rock properties may influence site response, wave propagation, soil–structure interaction, and the confinement condition of the tunnel lining. These factors may further modify the structural response and the fitted IM–response relationship. Accordingly, when the proposed framework is applied to tunnels with different burial depths or surrounding-medium conditions, the regression coefficients and recommended IM combinations should be further validated and recalibrated.

Compared with tunnel burial depth and surrounding-medium conditions in the present prescribed-input test, fault geometry may have a more direct influence on the applicability of the proposed framework. In particular, a change in fault dip angle may modify the projection of fault-induced relative displacement and velocity onto the local tunnel coordinate system, the spatial extent of the fault-crossing zone, and the dominant deformation component of the tunnel lining. Similarly, the tunnel–fault intersection angle may affect the relative contributions of longitudinal, transverse, and vertical deformation components. Therefore, although the relative-motion-based IM concept remains physically applicable, the fitted coefficients, empirical PGD/PGV threshold, and dominant response component may vary with fault geometry. Further validation considering different fault dip angles and oblique fault-crossing configurations is required before generalizing the proposed framework to broader fault-crossing tunnel scenarios.

Another limitation is related to the selection of the structural response metric. In this study, peak lining strain was adopted as the primary response quantity because it was directly measured at multiple monitoring sections and can effectively characterize the local deformation demand of the tunnel lining near the fault-crossing zones. In addition, the shaking table input motions did not include an axial seismic excitation component along the tunnel axis. Therefore, complex coupled deformation modes involving both bending and axial deformation were not the focus of the present experimental program. Nevertheless, the effectiveness of different IMs may depend on the selected response quantity. Other response metrics, such as curvature, joint opening, joint rotation, differential settlement, acceleration response, or localized cracking, may be governed by different deformation mechanisms and may exhibit different correlations with the proposed relative-motion-based IMs. Therefore, the conclusions obtained from peak lining strain should be interpreted within the scope of the present response metric, and further studies are needed to examine whether the proposed IM framework remains applicable when other damage or performance indicators are considered.

The sequential multi-level loading protocol adopted in the shaking table tests is another source of uncertainty. To monitor the structural state during the loading sequence, white-noise sweep tests were conducted before each seismic intensity level to identify the dynamic characteristics of the integrated tunnel–surrounding rock model. The results showed that the natural frequency did not exhibit a continuous or significant decrease after the lower-intensity excitation levels, indicating that no obvious irreversible stiffness degradation occurred during the early low-level loading stages.

In addition, after each graded seismic loading level was completed, high-definition cameras installed inside the model were used to inspect critical regions of the tunnel lining, including the crown, spandrels, sidewalls, and flexible joints. No visible cracking, surface spalling, joint dislocation, interface debonding, or other obvious damage was observed after the low-intensity earthquake level. These observations suggest that the lower-level excitations did not significantly compromise the structural integrity of the model before subsequent higher-level loading tests.

Nevertheless, minor internal micro-damage or material property evolution under repeated seismic loading cannot be completely excluded. Since peak lining strain is sensitive to stiffness degradation and local damage, possible cumulative damage may slightly amplify the strain response under subsequent higher-level excitations and influence the fitted IM–response relationships. Therefore, the correlation results obtained in this study should be interpreted within the context of the adopted sequential multi-level loading protocol, rather than as the response of a completely undamaged specimen subjected to a single independent excitation. Future studies should consider refined numerical simulations or independent specimens under single-level loading to further quantify the influence of damage accumulation.

Finally, although an internal validation analysis was conducted using moderate-earthquake data that were not involved in the fitting of the multi-IM regression surfaces, all validation data were still obtained from the same shaking table test program. Therefore, the validation results provide evidence for the predictive capability of the proposed framework within the present experimental conditions, but they should not be interpreted as external validation for all fault-crossing tunnel scenarios. No independent numerical simulation was conducted in the present study to externally validate the fitted IM–response relationships; therefore, further numerical validation is required before extending the proposed framework to other tunnel configurations.

6. Conclusions

Based on the shaking table test results and the systematic evaluation of ground-motion intensity measures for fault-crossing tunnels, the following conclusions are drawn:

1. Fault-crossing tunnel response is governed by fault-induced relative deformation rather than by inertial demand alone. Absolute-motion-based intensity measures are inadequate for providing stable response ranking or strong correlation with tunnel lining strain demand, regardless of whether seismic mitigation measures are applied.
2. Relative-motion-based intensity measures are essential for characterizing seismic demand in fault-crossing tunnels, but no single measure is sufficient. Ratio-type relative IMs such as PGD/PGV effectively distinguish the relative severity of different ground-motion cases, whereas displacement-based relative IMs better capture response magnitude, revealing an inherent trade-off when using a single descriptor.
3. Within the range of the present shaking table test data, the multi relative-motion-based IM framework shows improved capability in characterizing tunnel lining strain response compared with single-IM formulations. By combining PGD/PGV with displacement-related relative IMs, such as I_D, CAD, and D_e, the proposed framework jointly reflects the deformation mechanism and the intensity level of fault-induced relative motion.
4. The comparison between the unmitigated and mitigated tunnel structures indicates that seismic mitigation mainly changes the response amplitude of the tunnel lining, while the dominant IM–response correlation pattern associated with fault-induced relative deformation remains broadly consistent within the present experimental dataset. This suggests that the proposed relative-motion-based IM concept is applicable to both tested lining configurations. However, the fitted coefficients and recommended IM combinations should be recalibrated when different tunnel configurations, mitigation systems, fault geometries, surrounding-medium conditions, or response indicators are considered.
5. The proposed multi-IM framework may provide a useful reference for ground-motion selection in fault-crossing tunnel analysis. PGD/PGV can be used to describe the deformation characteristics of candidate motions, whereas displacement-related relative IMs can be used to represent the intensity level of fault-induced relative movement. However, the empirical threshold and recommended IM combinations obtained in this study should be interpreted within the scope of the present input motions and require further validation before direct application to broader engineering conditions.

CRediT authorship contribution statement

Chao Luo: Writing – original draft, Methodology, Funding acquisition, Conceptualization. **Haowei Du:** Writing – original draft, Visualization, Software, Data curation. **Yanliang Du:** Supervision, Resources, Project administration, Funding acquisition. **Xiangbo Bu:** Writing – review & editing, Validation, Investigation. **Fei Xu:** Writing – review & editing, Resources, Funding acquisition. **Hemin Zheng:** Funding acquisition. **Hao Wang:** Writing – review & editing, Funding acquisition. **Zerui Ji:** Investigation.

Declaration of competing interest

The authors declare that they have no known competing financial interests or personal relationships that could have appeared to influence the work reported in this paper.

Acknowledgments

This work was supported by the National Key Research and Development Program of China (Grant Nos. 2025YFF0519000, 2025YFF0519001); the National Natural Science Foundation of China (Grant Nos. 52478407, 52427813); the Science and Technology Research and Development Platform Special Project of Hebei Province (Grant Nos. 25361702D, 25365407D); the S&T Program of Hebei (Grant Nos. 254Z5402G, 232A7601Z), the Natural Science Foundation of Hebei Province (CN) (Grant No. E2024210049); the Scientific Research Project of Higher Education Institutions in Hebei Province (Grant No. CXZX2025050); the Key Research and Development Plan of Yunnan Provincial Science and Technology Department (Grant No. 202303AA080005); the Earthquake Science and Technology Program of Hebei Province (Grant No. DZ2025092800001) and the Class A Key Project of China Railway Design Group (Grant No. 2023A0103601).

The authors gratefully acknowledge the support provided by the *Earthquake Engineering Research & Test Center of Guangzhou University* during the shaking table tests. Special thanks are extended to Professor Xiangyun Huang, Mr. Jianqiu Chen, and Dr. Ying Zhang for their valuable assistance. The authors also appreciate the help of other research and technical staff members who contributed to the experimental work.

Data availability

Data will be made available on request.

References

Arias, A., 1970. A measure of earthquake intensity. In: Press, M.I.T. (Ed.), Seismic Design for Nuclear Power Plants. Massachusetts, Cambridge, pp. 438–483.

Baker, J.W., 2007. Correlation of Ground Motion Intensity Parameters Used for Predicting Structural and Geotechnical Response. Presented at the Tenth international conference on application of statistics and probability in civil engineering, Taylor & Francis Group, p. 115.

Baker, J.W., Jayaram, N., 2008. Correlation of spectral acceleration values from NGA ground motion models. Earthq. Spectra 24, 299–317. https://doi.org/10.1193/1.2857544.

Bray, J.D., Travasarou, T., 2007. Simplified procedure for estimating earthquake-induced deviatoric slope displacements. J. Geotech. Geoenviron. Eng. 133, 381–392. https://doi.org/10.1061/(ASCE)1090-0241(2007)133:4(381).

Cornell, C.A., 1968. Engineering seismic risk analysis. Bull. Seismol. Soc. Am. 58, 1583–1606. https://doi.org/10.1785/BSSA0580051583.

Cornell, C.A., Jalayer, F., Hamburger, R.O., Foutch, D.A., 2002. Probabilistic basis for 2000 SAC federal emergency management agency steel moment frame guidelines. J. Struct. Eng. 128, 526–533. https://doi.org/10.1061/(ASCE)0733-9445(2002)128:4(526).

Gehl, P., Seyedi, D.M., Douglas, J., 2013. Vector-valued fragility functions for seismic risk evaluation. Bull. Earthq. Eng. 11, 365–384. https://doi.org/10.1007/s10518-012-9402-7.

Graves, R., 2022. Using a grid-search approach to validate the graves–pitarka broadband simulation method. Earth Planets Space 74, 186. https://doi.org/10.1186/s40623-022-01742-y.

Graves, R., Pitarka, A., 2015. Refinements to the graves and Pitarka (2010) broadband ground-motion simulation method. Seismol. Res. Lett. 86, 75–80. https://doi.org/10.1785/0220140101.

Graves, R.W., Pitarka, A., 2010. Broadband ground motion simulation using a hybrid approach. Bull. Seismol. Soc. Am. 100, 2095–2123. https://doi.org/10.1785/0120100057.

Hadiani, N., Davoodi, M., Jafari, M.K., 2013. Correlation between settlement of embankment dams and ground motion intensity indices of pulse-like records. iranian journal of science and technology. Trans. Civil Eng. 37, 111–126.

Hashash, Y.M.A., Hook, J.J., Schmidt, B., Yao, J.-I.-C., 2001. Seismic design and analysis of underground structures. Tunn. Undergr. Space Technol. 16, 247–293. https://doi.org/10.1016/S0886-7798(01)00051-7.

Iervolino, I., Cornell, C.A., 2005. Record selection for nonlinear seismic analysis of structures. Earthq. Spectra 21, 685–713. https://doi.org/10.1193/1.1990199.

Karamitros, D.K., Bouckovalas, G.D., Kouretzis, G.P., 2007. Stress analysis of buried steel pipelines at strike-slip fault crossings. Soil Dyn. Earthq. Eng. 27, 200–211. https://doi.org/10.1016/j.soildyn.2006.08.001.

Luco, N., Cornell, C.A., 2007. Structure-specific scalar intensity measures for near-source and ordinary earthquake ground motions. Earthq. Spectra 23, 357–392. https://doi.org/10.1193/1.2723158.

Luo, C., Cao, X., 2024. Applicability study of the GP Fault rupture model in strong ground motion simulation for the qinghai menyuan Ms6.9 earthquake. Chinese J. Geophysics (in Chinese) 67, 534–547. https://doi.org/10.6038/cjg2023Q0695.

Mackie, K.R., 2004. Fragility-based seismic decision making for highway overpass bridges. University of California, Berkeley.

Moehle, J., Deierlein, G.G., 2004. A framework methodology for performance-based earthquake engineering. In: Vancouver, B.C. (Ed.), Presented at the 13th World Conference on Earthquake Engineering. Canada, pp. 679–692.

Nau, J.M., Hall, W.J., 1984. Scaling methods for earthquake response spectra. J. Struct. Eng. 110, 1533–1548. https://doi.org/10.1061/(ASCE)0733-9445(1984)110:7(1533).

Nguyen, V.-Q., Roh, H., Park, D., 2023. Optimal earthquake intensity measures for probabilistic seismic demand models of rectangular tunnels. In: Smart Geotechnics for Smart Societies. CRC Press, London, pp. 1574–1579. https://doi.org/10.1201/9781003299127-231.

O'Rourke, M.J., Liu, X., 2012. Seismic design of buried and offshore pipelines. MCEER Monograph, Multidisciplinary Center for Earthquake Engineering Research, Buffalo, NY, USA.

Penzien, J., 2000. Seismically induced racking of tunnel linings. Earthq. Eng. Struct. Dyn. 29, 683–691. https://doi.org/10.1002/(SICI)1096-9845(200005)29:5%3C683::AID-EQE932%3E3.0.CO;2-1.

Petrone, F., Abrahamson, N., McCallen, D., Pitarka, A., Rodgers, A., 2021. Engineering evaluation of the EQSIM simulated ground-motion database: The san francisco bay area region. Earthquake Eng. Structural Dynamics 50, 3939–3961. https://doi.org/10.1002/eqe.3486.

Pitarka, A., Graves, R., Irikura, K., Miyakoshi, K., Rodgers, A., 2020. Kinematic rupture modeling of ground motion from the M7 kumamoto. Japan Earthquake. Pure Appl. Geophys. 177, 2199–2221. https://doi.org/10.1007/s00024-019-02220-5.

Rodgers, A.J., Pitarka, A., Pankajakshan, R., Sjogreen, B., Petersson, N.A., 2020. Broadband (0-10 Hz) 3D simulations of Mw 7 hayward fault earthquakes with site response corrections. Bull. Seismol. Soc. Am. 110, 2862–2881. https://doi.org/10.1785/0120200147.

Shen, Y., El Naggar, M.H., Zhang, D., Huang, Z., Du, X., 2025. Scalar- and vector-valued seismic fragility assessment of segmental shield tunnel lining in liquefiable soil deposits. Tunn. Undergr. Space Technol. 155, 106171. https://doi.org/10.1016/j.tust.2024.106171.

Shen, Y., El Naggar, M.H., Zhang, D., Huang, Z., Du, X., 2025. Optimal intensity measure for seismic performance assessment of shield tunnels in liquefiable and non-liquefiable soils. Underground Space 21, 149–163. https://doi.org/10.1016/j.undsp.2024.03.008.

Trifunac, M.D., Brady, A.G., 1975. A study on the duration of strong earthquake ground motion. Bull. Seismol. Soc. Am. 65, 581–626.

Tsinidis, G., 2017. Response characteristics of rectangular tunnels in soft soil subjected to transversal ground shaking. Tunn. Undergr. Space Technol. 62, 1–22. https://doi.org/10.1016/j.tust.2016.11.003.

Vamvatsikos, D., Cornell, C.A., 2005. Developing efficient scalar and vector intensity measures for IDA capacity estimation by incorporating elastic spectral shape information. Earthquake Engng Struct. Dyn. 34, 1573–1600. https://doi.org/10.1002/eqe.496.

Wang, J.-N., 1993. Seismic design of tunnels: A simple state-of-the-art design approach. Parsons Brinckerhoff Quade & Douglas Inc, New York, NY.

Wells, D.L., Coppersmith, K.J., 1994. New empirical relationships among magnitude, rupture length, rupture width, rupture area, and surface displacement. Bull. Seismol. Soc. Am. 84, 974–1002. https://doi.org/10.1785/BSSA0840040974.

Xu, F., Bu, X., Du, Y., Luo, C., Zheng, H., Liu, X., Gu, Q., 2026. Shaking table tests on tunnels crossing multiple faults incorporating dislocation-ground motion coupling. Experimental System and Implementation. Tunnelling and Underground Space Technology (Under Review).

Xu, Y., Lu, X., Tian, Y., Huang, Y., 2022. Real-time seismic damage prediction and comparison of various ground motion intensity measures based on machine learning. J. Earthq. Eng. 26, 4259–4279. https://doi.org/10.1080/13632469.2020.1826371.

Zhang, C., Zhao, M., Zhong, Z., Du, X., 2023. Optimal intensity measures in probabilistic seismic demand model of subway station. Tunn. Undergr. Space Technol. 142. https://doi.org/10.1016/j.tust.2023.105443.